Economic Geology
Vol. 84, 1989, pp. 2115–2138

Ledge Formation at the Sandstorm and Kendall Gold Mines, Goldfield, Nevada

PETER G. VIKRE

ASARCO Inc., 510 East Plumb Lane, Reno, Nevada 89502

Abstract

Gold ore at the adjacent Sandstorm and Kendall mines occurs in silicified fissures or ledges that formed by both open-space deposition and replacement of Miocene rhyolites 2 mi (3.2 km) north of Goldfield, Esmeralda County, Nevada. The ledges, which are approximately 21 Ma, alteration selvages, and volcanic stratigraphy at Sandstorm-Kendall are similar to those of the main district, immediately northeast of the town of Goldfield, where more than 95 percent of past gold production occurred. From 1903 to 1947 4.2 M oz (136,360 kg) of gold was produced from the Goldfield district.

En echelon Sandstorm-Kendall ledge segments consist of six assemblages which from oldest to youngest are: (1) ledge replacement quartz, (2) barite + sulfides, (3) quartz + pyrite + barite, (4) quartz + barite + kaolinite breccia, (5) vuggy quartz, and (6) lateral replacement quartz. A large range in homogenization temperatures (292°–100°C), salinities (0.2–7.9 wt % NaCl), isotopic compositions (δD, +3 to −137‰; δ^{18}O, +4.2 to −17.6‰) and gas concentrations (3.8–27.5 wt % $CO_2 + H_2S + SO_2 + N_2$) is observed in quartz and barite of the six assemblages. Isotopic temperatures calculated for $\delta^{34}S_{pyrite\text{-}alunite}$ and $\delta^{34}S_{pyrite\text{-}gypsum}$ in wall-rock mineral assemblages range from 200° to 356°C.

Gold occurs as inclusions in copper sulfosalts (mainly luzonite and famatinite) and barite of assemblage (2), and in quartz and barite of assemblage (4). It is analytically detectable in assemblages (1) and (3). Rhyolites enclosing the six assemblages are altered to quartz + kaolinite or alunite adjacent to ledge segments, and to illite and montmorillonite-dominated zones with distance from the ledge. Quartz and kaolinite are the stable silicates in the ledge.

According to fluid isotope compositions and salinities, assemblages (1), (2), and (3) precipitated from heavy, pre-Miocene formation water, probably modified seawater, mixed with Miocene meteoric and magmatic water. Assemblage (4) was deposited by pre-Miocene formation water that either mixed with magmatic water or was enriched in δ^{18}O by exchange with Paleozoic metasedimentary rocks that underlie Goldfield. Assemblage (5) largely precipitated from Miocene meteoric water. Assemblage (6) fluid, which laterally replaced extensive volumes of andesite with quartz, is also Miocene meteoric water, but silicified andesite beneath laterally replaced andesite formed from δ^{18}O-enriched pre-Miocene formation water or increments of magmatic water. Sulfur isotope compositions permit derivation of barite from underlying Paleozoic metasedimentary rocks, which contain bedded barite deposits elsewhere in southwestern Nevada, and sulfide sulfur from Tertiary intrusions. Small amounts of organic matter in barite may also have been derived from Paleozoic rocks.

Spheroidal weathering of andesite preserved by assemblage (6) quartz and limited erosional exposure of andesite prior to mineralization indicate that ledge segments in the Sandstorm-Kendall area may have formed within hundreds of feet below the paleosurface. However, ledge fluid inclusion temperatures exceeding several hundred degrees centigrade at such shallow depths require a combination of thicker premineralization cover, fault displacements, lithostatic pressure, and more thorough evaluation of fluid inclusion phase ratios and gas compositions.

Distinguishing features of Sandstorm-Kendall ledge formation—near-surface fluid inclusion temperatures exceeding 250°C, high-temperature gradients, disparate and distal water sources, internal ledge brecciation and sedimentation, and gas-rich fluids containing $H_2S + SO_2$—are consistent with rapid, very shallow emplacement of magma beneath Goldfield. Since ledges are essentially coeval with rhyodacite, latite, and andesite in the main district, subvolcanic intrusions or diapirs of these rocks probably supplied thermal energy for mineralization both there and at Sandstorm-Kendall.

Introduction

THE gold deposits of Goldfield, Esmeralda County, Nevada, occur in intensely altered Miocene volcanic rocks. Ores mined from irregular, silica ledges during the 15 years following discovery in 1902 averaged >1 oz gold per ton. Production from the district was 4.2 M oz (136,360 kg) gold, 1.5 M oz (48,700 kg) silver, and 7.7 M lb (3.5 M kg) of copper from 7.7 million tons (7.0 million metric tons) of ore for the

0361-0128/89/1013/2115-24$3.00

period 1903 to 1947 (Albers and Stewart, 1972). Virtually all ore was recovered within a 0.5-mi^2 (1.25-km^2) area that borders the town of Goldfield to the northeast. This area is referred to hereinafter as the "main district." Small production totaling at least 60,000 oz Au was derived from satellite deposits 2 to 4 mi (3.2–6.4 km) north and northeast of Goldfield, including the Sandstorm and Kendall mines (Fig. 1) where gold in the district was initially discovered. Geology, structure, and hydrothermal mineral assemblages in the main district have been previously described (Ransome, 1909; Albers and Stewart, 1972; Ashley, 1974), but paragenetically controlled studies of minerals and ore fluids have been precluded by the fine-grain size and structural complexity of ores. Ledges in the Sandstorm-Kendall vicinity, however, contain coarse-grained, open-space-deposited phases that record a reasonably clear paragenesis. This paper presents data pertinent to hydrothermal evolution of ledges at the Sandstorm-Kendall mines. It also briefly compares ore formation at Sandstorm-Kendall to that in the main district and to that of the similar gold deposit at Summitville, Colorado.

Geology of the Sandstorm-Kendall Area

Rocks in the vicinity of the Sandstorm and Kendall mines include Jurassic quartz monzonite and Miocene rhyolites and andesite. Unconsolidated Tertiary-Quaternary sediment and mine dumps thinly cover the Miocene rocks (Fig. 2).

Cospatial, intercalated rhyolite tuff and flows, the Morena and Sandstorm rhyolites, respectively, of Ransome (1909) and the Sandstorm Formation of Albers and Stewart (1972) unconformably overlie quartz monzonite 2,500 ft (0.8 km) south from the Sandstorm shaft (Fig. 2). Alunitized quartz monzonite on the Sandstorm, Kendall, and other mine dumps indicates that the rhyolites aggregate no more than several hundred feet in thickness and that quartz monzonite underlies the entire Tertiary section shown in Figure 2. Unconformably overlying the rhyolites is Milltown Andesite (Ransome, 1909), which is less than 100 ft (<30 m) thick in the Sandstorm-Kendall area. It rarely crops out and is largely confined to predepositional depressions in rhyolite, except for Kendall Mountain (Fig. 2) which is capped by a large mass of silicified Milltown Andesite. Radiometric ages for Tertiary rocks are given in Table 1.

Numerous ledges, shafts, prospect pits, and trenches occur in Tertiary rocks. Virtually all productive segments of the Sandstorm-Kendall ledge are confined to rhyolite flows (Sandstorm rhyolite of Ransome, 1909). Some low-grade gold mineralization near the Adams and Conqueror shafts was mined from open pits along the Adams-Conqueror fault zone which separates rhyolite and Milltown Andesite (Fig. 2).

Ledges consist of semilinear zones of rhyolite replaced by very fine grained quartz (avg ~0.02 mm) in which some volcanic textures are preserved but only the relict minerals, quartz, zircon, and rutile, remain. The erosionally resistant ledges mark fissures and fault zones in Tertiary rocks, although displacement along faults is minor both at Sandstorm-Kendall and in the main district (Ransome, 1909). The east-dipping Adams-Conqueror fault zone (Fig. 2) has been considered the northern extension of the "Columbia Mountain fault" (Ransome, 1909; Searls, 1948). Displacement along this fault zone in the main district cannot be accurately determined, but the western breaks display no more than a few tens of feet of normal movement in the Sandstorm-Kendall area. In the main district much early importance was assigned to the Columbia Mountain fault as the western limit of ore, the source of ore solutions, and the ring fracture of a caldera. However, ore occurs west of this fault at the Sandstorm and Kendall mines and ore was also found in the 1940s west of the fault in the main district (Searls, 1948).

Regionally, the Sandstorm-Kendall area is situated on the northwestern flank of a volcanic dome that is cored by Jurassic quartz monzonite and Paleozoic metasedimentary rocks. The dome may have formed by several episodes of uplift related to caldera formation (Ransome, 1909; Ashley, 1974). It lies within a hypothesized ring fracture zone along which intrusive sources for all Goldfield premineralization eruptive rocks are situated (Ashley, 1974).

The Sandstorm-Kendall Ledge

The Sandstorm and Kendall mines are in a north–south–trending ledge which is about 1,000 ft (300 m) in length, 20 to 70 ft (6–21 m) wide, and dips 50° to 70° east. In the following discussion, numerous ledge segments that are en echelon to and along strike from the ledge segment in which the Sandstorm and Kendall shafts were sunk are considered part of the Sandstorm-Kendall ledge (Fig. 2).

Production from the Sandstorm mine was approximately 12,000 oz gold as estimated from Ransome (1909); mine dumps shown in Ransome's (1909) plate XIII photograph are no larger today. Kendall mine production, at least 5,000 oz as estimated from Ransome (1909), was undoubtedly expanded in subsequent years as the dumps are larger today and contain abundant unoxidized ledge material that was unavailable to Ransome. It may total 22,000 oz Au (M. Hamilton, pers. commun.). Small amounts of ore are reported to have averaged >200 oz Au/ton and most stoping apparently took place within 80 ft of the surface (Ransome, 1909). The ledge is composed mainly of dense, fine-grained quartz, which locally displays the texture of leached porphyritic and flow-banded rhyolite. Pockets of kaolinite, iron oxides, vuggy

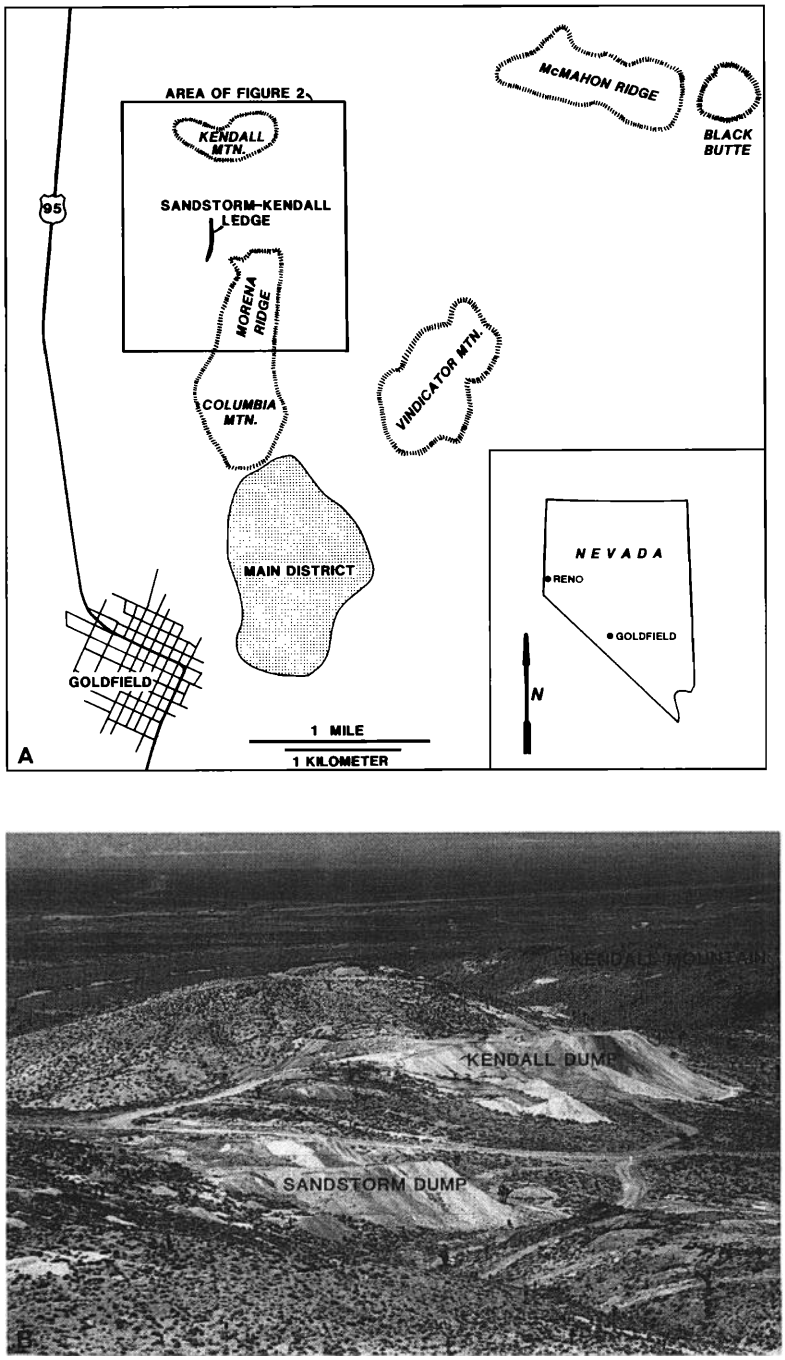

FIG. 1. A. Index map for the Goldfield district, Esmeralda County, Nevada, showing the main district, Sandstorm-Kendall ledge, and area covered in this paper (Fig. 2). B. Photograph, with view toward the north, of the Sandstorm and Kendall dumps, and Kendall Mountain.

quartz, and barite constitute ore-grade portions of the ledge and some ore was related by miners to transverse fissures cutting the ledge (Ransome, 1909). Numerous subparallel ledges adjacent to the Sandstorm-Kendall ledge were prospected but did not produce significant ore (Fig. 2).

Hydrothermal mineral assemblages

Hydrothermal minerals comprising the Sandstorm-Kendall ledge can be organized into six assemblages which include both quartz replacement of rhyolite flows and open-space precipitation of minerals in fis-

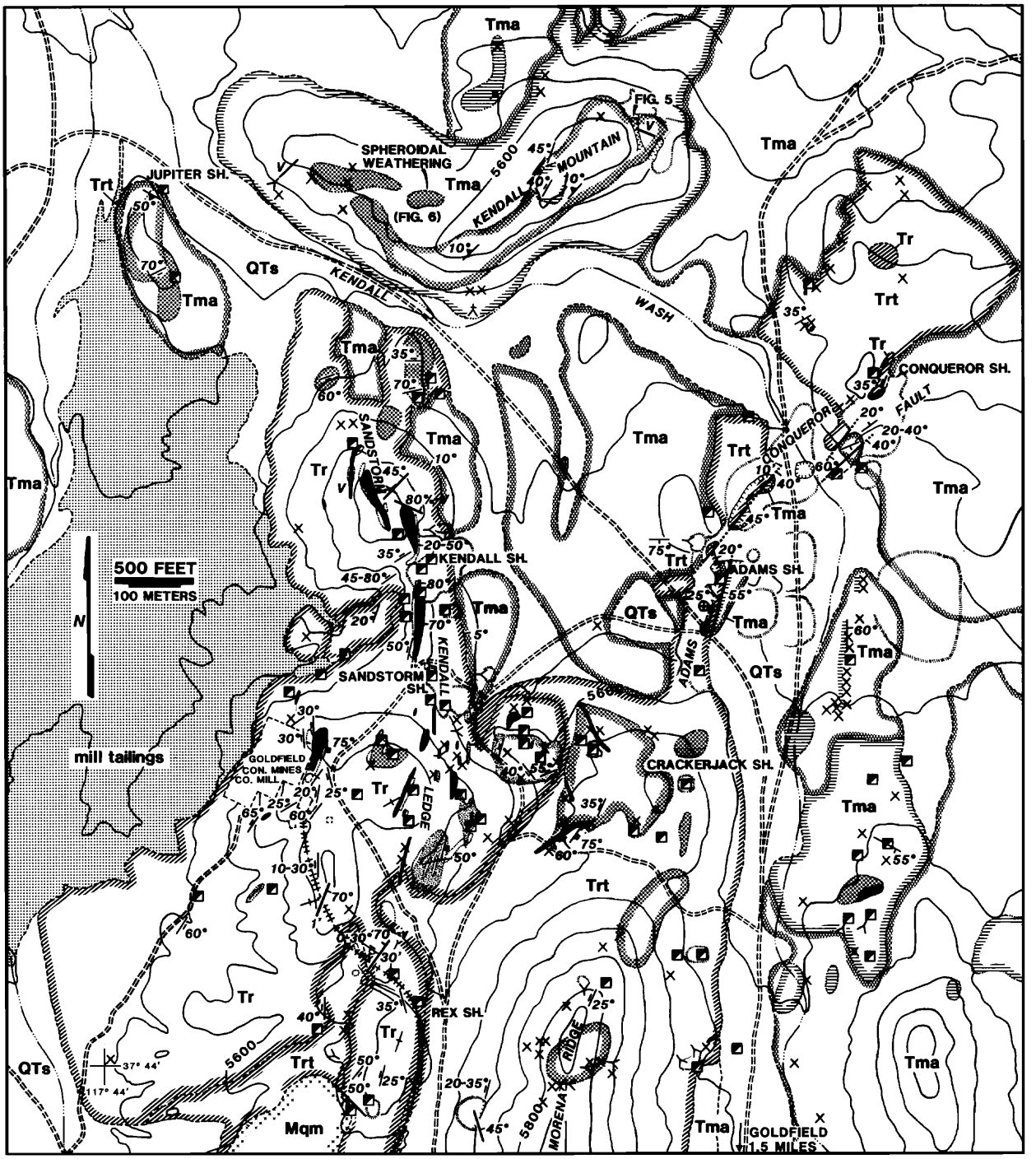

FIG. 2. Geology and hydrothermal alteration of the Sandstorm-Kendall area.

sures. Assemblages (1), (4), (5), and (6) were observed in place whereas the paragenesis of assemblages (2) and (3) relative to the other assemblages was determined from dump samples.

The edges of the ledge, and earliest assemblage, are porous to dense, completely silicified rhyolite in which most feldspars, phenocrysts, and matrix have been replaced by quartz. Feldspars in some silicified rhyolite have been removed but not replaced, leaving a vuggy, leached rock composed entirely of quartz. Quartz phenocrysts, flow foliation, and porphyritic texture are commonly preserved and 1 to 3 percent

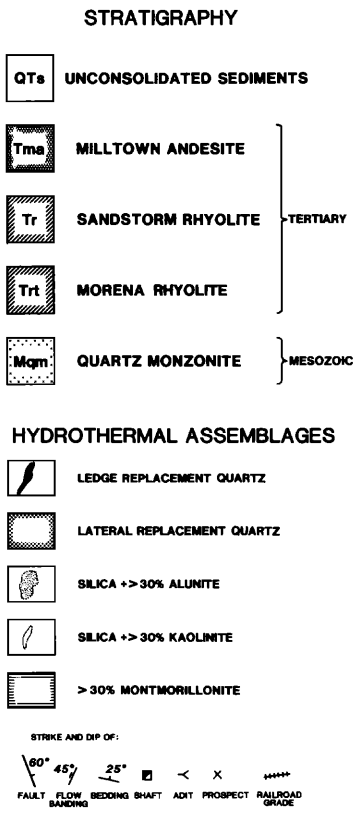

FIG. 2. Key

pyrite has been added to the rock. This assemblage (1), referred to hereafter as ledge replacement quartz, forms 60 to 100 percent of the ledge.

Some rhyolite parted across and along flow foliations creating numerous open spaces. The voids filled with alternating, banded, and crustified layers of quartz, pyrite, copper sulfosalts, barite, bismuthinite, gold, and kaolinite. These minerals comprise the second assemblage, hereafter referred to as the barite + sulfides assemblage, after the volumetrically important phases. Late within the second assemblage are lithified sediments consisting of quartz, kaolinite, and pyrite which filled some remaining open spaces.

The second assemblage has an intricate paragenesis. Barite euhedrons, often exceeding 1 in. (2.5 cm) in height, nucleated in many instances directly on massive replaced or vuggy leached rhyolite. Elsewhere, several-centimeter-thick bands of copper sulfosalts, bismuthinite, and pyrite, alternating with layers of fine-grained druzy quartz, cover silicified rhyolite surfaces and fragments. The final, hydrothermally precipitated layer within the second assemblage is invariably druzy quartz, opposing crystals of which sometimes coalesce in the centers of voids.

Gold occurs as inclusions in ledge replacement quartz of assemblage (1) and in copper sulfosalts and in barite of assemblage (2). Gold (and pyrite) inclusions in barite are often in the growth planes 001 and 210 (Fig. 3).

Chemical compositions for gold, sphalerite, and various Ag-, Cu-, Sb-, As-, Bi-, Sn-, Te-, Se-, and S-bearing phases from the Sandstorm-Kendall ledge and mine dumps elsewhere in the district are given in Table 2. These microprobe analyses and optical examinations of polished sections of opaque minerals from the Sandstorm-Kendall and several main district ledges reveal numerous sulfur-rich phases. Some have

TABLE 1. Radiometric Ages of Rocks and Ledges in the Sandstorm-Kendall Area

Sample no.	Unit	Mineral	Method	Age (Ma)	Source
GF87-5	Sandstorm Formation[1] (near Conqueror shaft)	Biotite	K-Ar	23.3 ± 0.7	This paper[3]
199-13	Sandstorm rhyolite[2]	Zircon	Fission track	28.6 ± 3.2	Ashley and Silberman (1976)
197-51-2	Kendall tuff[2]	Apatite	Fission track	31.1 ± 3.5	Ashley (1973)
197-51-2	Kendalll tuff[2]	Zircon	Fission track	33.2 ± 2.6	Ashley and Silberman (1976)
222-36	Morena rhyolite[1]	Sanidine	K-Ar	24.4 ± 0.5	Ashley and Silberman (1976)
222-36	Morena rhyolite[1]	Apatite	Fission track	27.7 ± 3.3	Ashley (1973)
222-36	Morena rhyolite[1]	Zircon	Fission track	31.1 ± 2.2	Ashley (1973)
97VV-229	Milltown Andesite	Hornblende	K-Ar	21.5 ± 0.5	Albers and Stewart (1972)
GF88-34	Milltown Andesite (roadcut, 1,000′ E of Morena Ridge)	Hornblende	$^{40}Ar/^{39}Ar$	18.7 ± 1.5	This paper[3]
GF88-35	Milltown Andesite (Jupiter dump)	Hornblende	$^{40}Ar/^{39}Ar$	23.4 ± 0.6	This paper[3]
GF86-1	Sandstorm-Kendall ledge (Sandstorm dump)	Alunite	K-Ar	21.6 ± 0.6	This paper[3]
GF87-1	Quartz monzonite (Alhambra dump)	Alunite	K-Ar	21.8 ± 0.8	This paper[3]
—	Average of five ledge samples from the main district, Preble Mountain, and Vindicator Mountain	Alunite	K-Ar	20.6 ± 0.8	Ashley and Silberman (1976)

[1] Unit designation of Albers and Stewart (1972)
[2] Unit designation of Ransome (1909)
[3] Analyses by E. H. McKee, Jr., U. S. Geological Survey, Menlo Park, California

TABLE 2. Chemical Analyses (wt %) of Minerals from the Sandstorm-Kendall Ledge, McMahon Ridge, and the Main District

Sample no.	Site	No. analyses	Location	Ag	Au	As	Bi	Cu	Fe	Sb	Sn	Se	S	Pb	Te	Zn	Cd	Mn	Sum	Approximate empirical stoichiometry	Probable mineral
Sandstorm-Kendall ledge																					
GFM85-1A	1	2	Kendall dump			13.47		46.88		5.33		0.11	31.85			0.68			98.33	$Cu_3Sb_{0.2}As_{0.7}S_4$	Luzonite
	2	2				1.18		48.54		18.53			32.75						101.00	$Cu_3Sb_{0.6}As_{0.1}S_4$	Famatinite
GFM85-1F	1	2				15.15		47.04		5.03			31.78		0.30	0.14			99.44	$Cu_3Sb_{0.2}As_{0.8}S_4$	Luzonite
	2	1				16.43		47.59		4.03			32.60		0.26	0.23			101.14	$Cu_3Sb_{0.1}As_{0.9}S_{4.1}$	Luzonite
McMahon Ridge																					
GF82-1B	1	2	Daisy dump						<0.04				34.67			65.40	0.36	<0.03	100.43	ZnS	Sphalerite
	2	2							<0.04				34.18			65.06	0.42	<0.03	99.66	ZnS	Sphalerite
	1	1		0.27						1.53			11.92	88.88					102.60	PbS	Galena
	1	1		1.84		2.55	0.79	35.19		10.82		0.84	25.70		17.31				95.04	$Cu_7(As_{0.4}Sb_{1.1})(Te_{1.7}S_{10})$	Goldfieldite (?)
	2	1		0.07		0.10	74.71	0.11		4.89		0.11	21.07						101.05	$Bi_{1.6}Sb_{0.2}S_3$	Goldfieldite (?)
Main district																					
GF81-2	1, 4	3	Grizzly Bear dump	1.33	98.75								0.74						100.82	$Au_{0.999}Ag_{0.001}$	Gold
	1, 3	2				10.12		45.11	3.43	16.58		0.84	25.49						101.57	$Cu_{3.6}(As_{0.7}Sb_{0.7})S_4$	Luzonite (?)
	1	1		0.50				75.63				0.28	19.52						96.34	Cu_2S	Chalcocite
	1, 2, 3, 5	5				9.11		46.33		14.44		0.83	29.15		0.41				100.23	$Cu_{3.2}(As_{0.5}Sb_{0.5})S_4$	Luzonite (?)
	3, 4	4		4.76				5.60		0.27		16.89	11.19		0.37				100.74	$Bi_{3.2}CuAg_{4.4}(Se_{2.3}S_{3.7})$	Luzonite (?)
							62.03														
GF81-4	1, 2, 3	10	Goldfield Consolidated	0.70	98.03														98.73	$Au_{0.98}Ag_{0.007}$	Gold
																			98.70	$Bi_{2.3}S_3$	Bismuthinite
	1	3	dump				80.92		0.67			0.56	16.58								
GF82-3A	2	1	Clermont dump	1.18	99.43								0.09						100.70	$Au_{0.99}Ag_{0.001}$	Gold
	3	1		0.37		2.29	1.96	40.65		1.71		0.48	28.20		25.46				101.12	$Cu_{12}(As,Bi,Sb)Te_4S_{17}$	Gold
	1	2		1.27	52.07							2.35	0.03		43.54				99.26	$(Au_{2.9}Ag_{0.1})(Te_{3.7}Se_{0.3})$	Gold
GF82-4	1	2	Mohawk mine,	0.54	99.72								0.10						100.36	$Au_{0.997}Ag_{0.005}$	Gold
	3	1	800–1,000	0.22			1.95	30.97	3.73	0.10	33.44	0.99	27.49						98.89	$Cu_7FeSn_4S_{12}$	Gold
	3	2	level	1.18		0.09	52.08	22.07	0.29	0.70	1.55	4.44	18.31		0.56				101.23	$Cu_8Bi_{11}(S_{1.9}Se)$	Gold
	4	1					83.63			0.48		0.10	17.08						101.29	$Bi_{2.3}S_3$	Bismuthinite
	1	1		1.23			76.76	2.25		0.31		6.64	13.95						101.14	$Bi_{2.8}Cu_{0.3}(S_{3.3}Se_{0.7})$	Bismuthinite
	1	1				3.43	1.85	42.89		11.89	0.09	0.40	25.51		15.09				101.15	$Cu_{7.4}(Sb_{1.1}As_{0.5})(S_{8.7}Te_{1.3})$	Goldfieldite
	2	1		1.96		13.20		39.17	3.23	12.92		0.43	26.17		0.08				97.88	$Cu_{2.6}Fe_{0.7}(Sb_{1.3}Ag_{6.4})S_{10}$	Goldfieldite
	2	1		0.30		11.21		43.87	0.08	11.44		0.07	30.43		1.24				98.64	$Cu_{2.9}(Sb_{0.4}As_{0.6})S_4$	Luzonite (?)
	5	1		0.27				35.32	5.53	0.13	29.34	0.58	29.94						101.11	$Cu_{11}Sn_5Fe_2S_{20}$	Luzonite (?)
GF87-15C	1, 2, 3	7	Mushett dump						<0.04				32.84			66.58	0.92	<0.03	100.34	ZnS	Sphalerite
	2, 5	5		0.65	99.62								0.09						100.36	Au	Gold
	2	2				9.85		47.40		12.17			30.91						100.33	$Cu_3Sb_{0.4}As_{0.5}S_{3.9}$	Luzonite
	2	2					85.51			0.83		0.52	16.89						103.75	$Bi_2S_{2.6}$	Bismuthinite

Compositions were determined at the University of Arizona by microprobe wave length analysis using pure elements and troilite as standards; where multiple analyses were obtained for individual minerals, element abundances varied generally <10 percent; stoichiometry based on single analyses is approximate

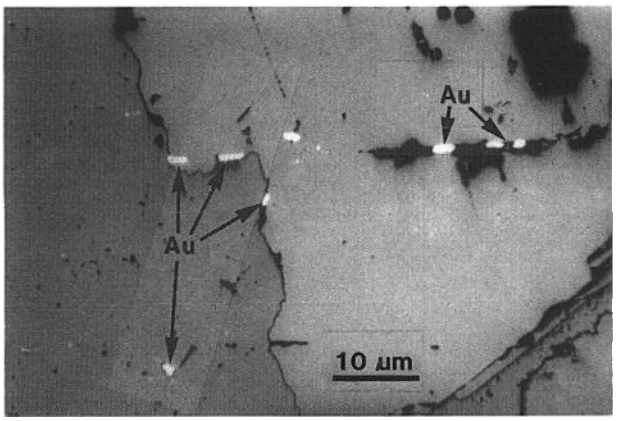

FIG. 3. Inclusions of gold in barite along a grain boundary (left) and along 001 (right).

atomic ratios that resemble no documented minerals, although their stoichiometry is based on few data. Where sphalerite is present (McMahon Ridge; Mushett lease in the main district), the FeS content is <0.07 mole percent. Gold compositions, $Au_{0.98}$ $Ag_{0.01}$ to $Au_{0.99}$ $Ag_{<0.01}$, vary little between main district and Sandstorm-Kendall ores. The most abundant copper mineral that occurs with barite and quartz at Sandstorm-Kendall has the optical properties and composition (Table 2) of enargite or luzonite, although appreciable antimony is present. XRD analyses of optically homogeneous samples indicate that both minerals are present, with luzonite predominating. In the main district Ransome (1909) considered famatinite to be prevalent whereas the composition of the most abundant Cu-Sb-As-S mineral is more nearly Cu_3 ($Sb_{0.5}$ $As_{0.5}$) S_4 (Table 2), somewhat intermediate between the isotype end members famatinite and luzonite.

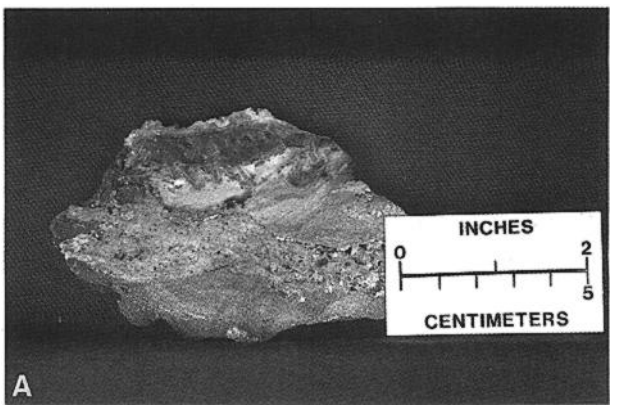

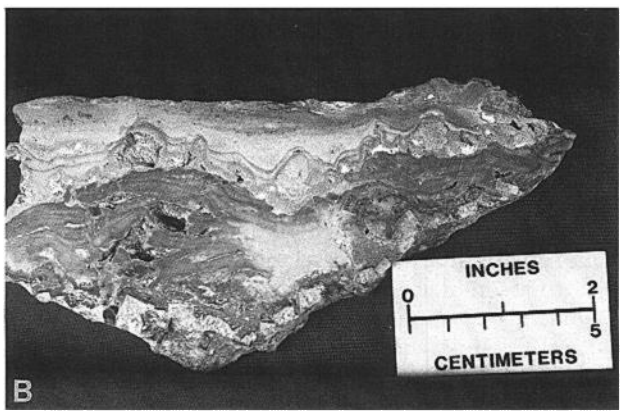

FIG. 4. Sedimentary beds within assemblage (2) of the Sandstorm-Kendall ledge.

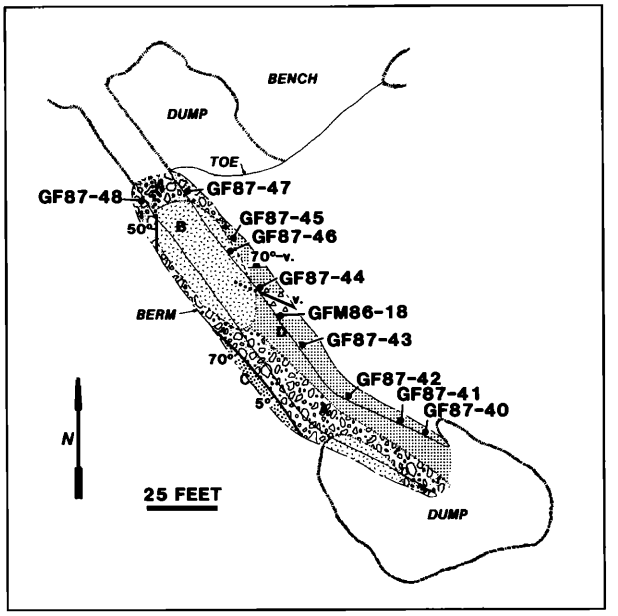

FIG. 5. Sketch map of a trench at the east end of Kendall Mountain (Fig. 2), showing alteration of Milltown andesite and isotope sample locations. A = irregularly sized, chaotically distributed blocks of silica in a soft, light brown matrix composed of kaolinite, quartz, and montmorillonite; both blocks and matrix at least partially retain the porphyritic texture of Milltown andesite, and contacts between blocks and matrix are gradational; some blocks are disrupted relative to the clay matrix and appear to have slumped. B = soft, light green, checked, microcrystalline aggregate of quartz and montmorillonite which has retained the porphyritic texture of Milltown andesite; in gradational contact with A and D. C = soft, light green, spheroidally weathered Milltown andesite, in fault contact with A. D = nearly massive, jointed quartz which locally retains the porphyritic texture of Milltown andesite; locally vuggy and contains 2 to 3 percent iron oxide or small dark patches of unoxidized pyrite; in gradational contact with A; comprises assemblage (6).

Clastic and chemical sediments occur locally within the second assemblage. These sediments are similar to those described by Schieber and Katsura (1986) for the Bohemia district (Oregon) veins. Unoxidized sediment consists of fine sand- to silt-textured tan and gray beds, <1 to 2 mm thick, containing local pockets

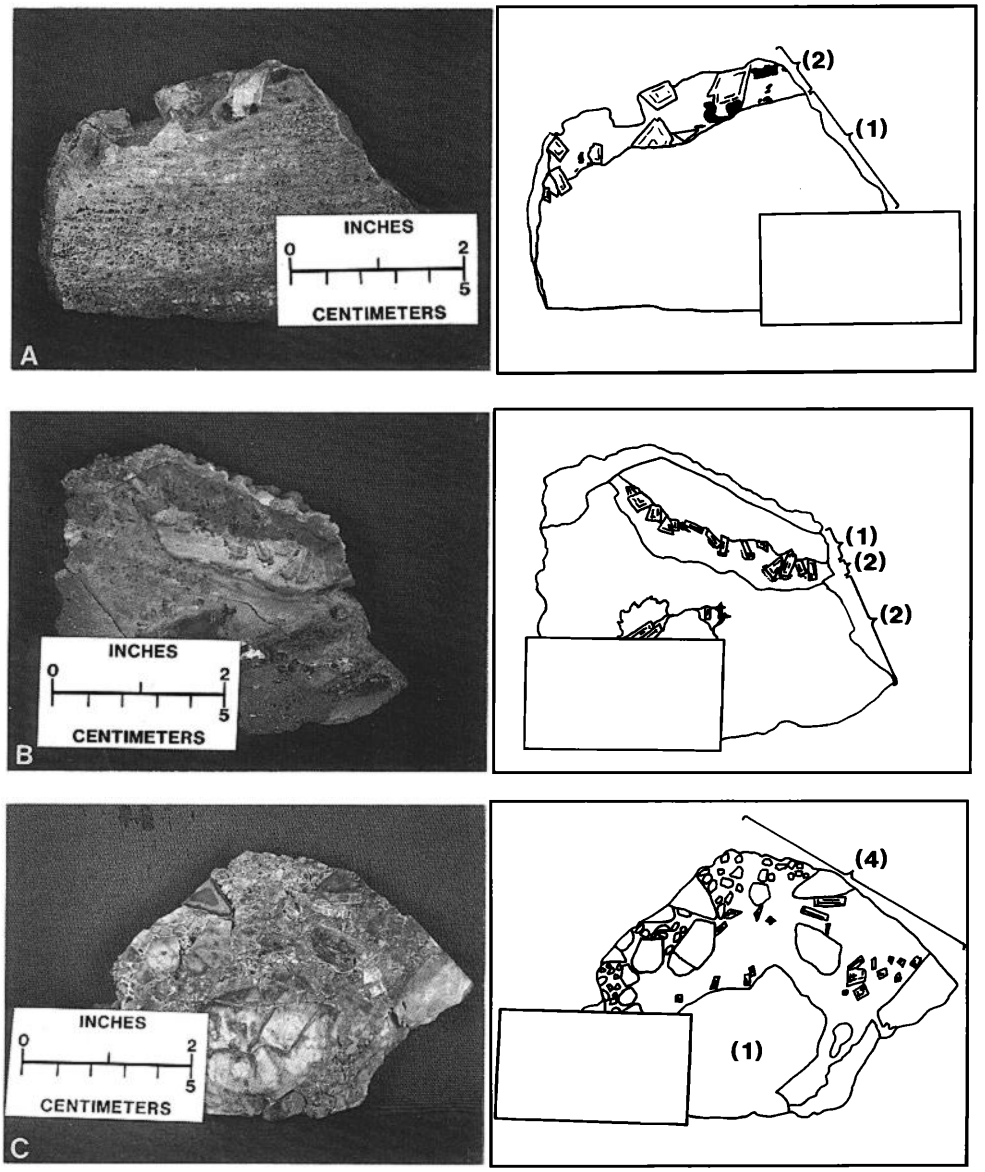

FIG. 6. Photographs and line drawings of assemblages within the Sandstorm-Kendall ledge. Numbers in parentheses refer to assemblages for which minor element analyses are given in Table 3. A. Silicified, porous, leached rhyolite of assemblage (1). Copper sulfosalts and barite euhedrons encrusted on the upper surface of assemblage (1) comprise assemblage (2). B. Clast of silicified rhyolite (assemblage (1)) covered with barite euhedrons and minor copper sulfosalts (assemblage (2)). Banded sediments of assemblage (2) comprise the remainder of the rock. Kaolinite pockets occur within the sediments. C. Silicified rhyolite clasts (assemblage (1)) cemented by quartz, barite, and kaolinite which constitute assemblage (4).

of kaolinite (Fig. 4). Clasts are quartz and pyrite. Thin <1-mm beds of microcrystalline quartz (averaging 0.05 mm), which may have precipitated from solution, are intercalated with clastic beds. The clastic beds drape over preexisting protuberances and are locally graded and crossbedded. The source of the sediment is unknown, but it probably originated and was transported in a manner similar to the quartz inclusions in assemblage (2) barite euhedrons described in a later section.

In the Kendall mine massive pyrite intergrown with subordinate quartz and barite euhedrons constitutes a third assemblage. This assemblage was not viewed in place, but dump samples show that it is paragenetically later than the second assemblage of barite + sulfides. Gold was not observed in polished section but was detected by assay (Table 3). Grain sizes of assemblage (3) minerals range from 2 mm to 1 cm and the minerals form subequigranular aggregates.

Apparently confined to within 80 ft of the surface

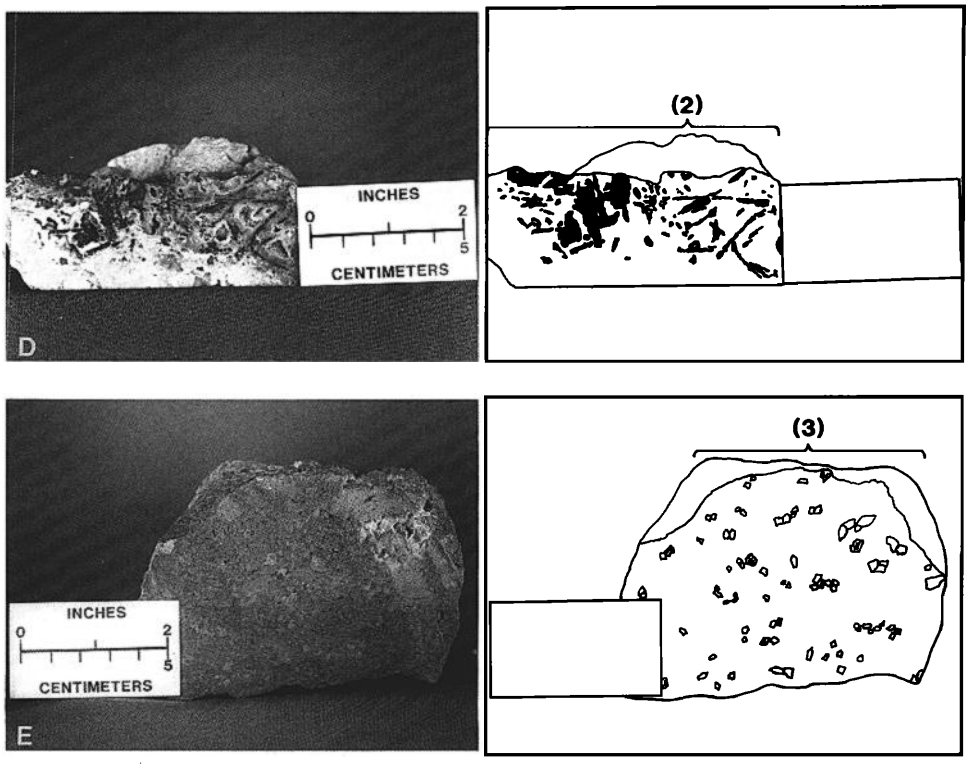

FIG. 6. (*Cont.*) D. Silicified, porous, leached rhyolite encrusted by copper sulfosalts of assemblage (2). E. Aggregate of quartz and pyrite subhedrons and barite euhedrons, constituting assemblage (3).

in the Sandstorm-Kendall ledge is a fourth assemblage which largely constitutes high-grade ore (Ransome, 1909). This assemblage is loosely compacted breccia consisting of completely silicified, angular, rhyolite fragments of assemblage (1) cemented by quartz, kaolinite, and coarse-grained barite. The breccia is nearly entirely oxidized, but remnant pyrite remains in some silicified clasts and in barite euhedrons. Gold is sporadically distributed both in the silicified clasts and barite crystals and also in kaolinite according to Ransome (1909). The coeval precipitation of barite and gold is indicated by gold inclusions in barite growth planes (Fig. 3). The relationship of assemblage (4) quartz + barite + kaolinite breccia to some earlier assemblages was not directly observed, but assemblage (4) is enclosed by the ledge replacement quartz, assemblage (1), in surface exposures. The quartz + barite + kaolinite breccia may be a coeval surface manifestation of the deeper assemblages (2) and (3).

In ledges in Sandstorm Formation rhyolite south of the Sandstorm shaft (Fig. 2), the repetitive barite-quartz-copper sulfosalts bands of the second assemblage are rare and ⅜-in. (1-cm) quartz euhedrons cover barite directly, forming crystal-lined pockets up to several feet in dimension. This vuggy quartz comprises a fifth assemblage. It also occurs locally in the Sandstorm and Kendall mines covering quartz + pyrite + barite of assemblage (3), thereby distinguishing assemblage (5) from sulfide-poor assemblage (2).

Kendall Mountain (Figs. 2 and 5) is an erosionally resistant ridge of Milltown Andesite, capped by 10 to 20 ft (3–6 m) of andesite which is nearly completely replaced by quartz and contains <3 percent pyrite. Beneath and within the silicified layer andesite is altered to light green, white, or brown aggregates of quartz, kaolinite, and montmorillonite. Relict porphyritic texture is well preserved in clay-altered andesite but is obscure in silicified andesite, although spheroidal weathering texture within silicified andesite is locally evident. The pervasively silicified andesite covering Kendall Mountain comprises the sixth assemblage, referred to as lateral replacement quartz.

Photographs of some Sandstorm-Kendall ledge assemblages are shown in Figure 6 with corresponding minor element analyses in Table 3.

Paragenesis

The relative ages of the ledge assemblages are incompletely known. Within the ledge, assemblages (2) through (5) are internal to and younger than assemblage (1) as determined from the sequential arrangement of the assemblages in outcrop and dump samples. The relationship of assemblage (2) to assemblage (3) was observed only in dump samples. Assemblage

TABLE 3. Selected Element Analyses of Assemblages within the Sandstorm-Kendall Ledge

Photograph letter[1] (Fig. 6)	Assemblage	Field number	Au	Ag	Cu	As	Sb	Te	Sn	Bi	Hg
			oz/ton					(ppm)			
A	(1)	GFM86-1C	0.09	1.0	178	74	86	20.3	58	65.0	27.0
		GFM85-1 eqa	0.02	0.1	270	79	18	4.8	12	17.1	7.37
B	(2)	GFM86-1E	0.09	4.6	2.1%	5,039	1,480	223	570	791	6,239
		GFM86-1D (barite + sulfides)	0.08	1.6	3,000	818	480	235	158	586	132
C	(2)	GFM85-1E (Sediments)	0.46	1.2	1,100	53	44	NA	1	NA	0.02
D	(4)	GFM86-1F	0.02	0.1	43	64	20	74.6	6	32.6	1.63
E	(2)	GFM86-1B	2.34	30.8	8.6%	1.85%	3,100	2,340	1,940	3,510	212
F	(3)	GFM86-1A	0.75	7.2	1,280	349	650	647	178	154	130

Analyses by Cone Geochemical, Inc., Lakewood, Colorado, and Hunter Mining laboratory, Sparks, Nevada; NA = not analyzed
[1] Photograph letters correspond to those in Figure 6

(4) does not occur deeper than about 100 ft below the surface (Ransome, 1909) and may be coeval with assemblages (2) and (3). Assemblage (5) covers assemblages (2) and (3) but was not observed in contact with assemblage (4). Assemblage (6) stratigraphically overlies all the other assemblages and isotopic data (see later section) suggest that it may be the same relative age as (5).

Barite history

Both microscopic and hand specimen examination of large barite crystals in assemblages (2), (3), and (4) reveal several growth-related events that involved physical as well as chemical perturbations in the fluid from which the barite crystallized. The barite euhedrons are either free standing and attached to the sides of vugs or are covered by quartz-pyrite sediments and copper sulfosalt crystals of assemblage (2), or quartz of assemblage (5). Both primary fluid inclusions and opaque and transparent solid inclusions (Fig. 3) were episodically incorporated along growth planes in the barite (Fig. 7). The transparent solid inclusions are exclusively spindle-shaped clasts of quartz which range in size from <1 to ~30 μm with a mean of ~10 μm. Inclusions along individual planes are moderately sorted with a grain size variation commonly ±5 μm. They resemble doubly terminated quartz euhedrons that have been physically abraded as crystal edges are rounded and not sharp. Some of the 001 and 210 barite growth planes containing denser quartz inclusions are megascopically visible as cloudy layers. The entrained quartz inclusions are invariably more abundant on one of the crystal growth planes (Fig. 8). In assemblage (2) where copper sulfosalts encrust barite euhedrons, the distribution of copper minerals is similarly skewed.

Other dense planes of amorphous black inclusions of possible organic matter were precipitated in growth planes near the cores of barite euhedrons (Fig. 7) and are preferentially oriented similarly to quartz inclusions. Irregular fractures that crosscut growth planes containing the amorphous black and quartz inclusions appear to be filled with similar black material. No compositional data were obtained for this phase. However, a similar, soft gray opaque phase with very low reflectivity which occurs with assemblage (2) quartz in a sample from the Kendall dump was semi-

TABLE 4. Ranges of Fluid Inclusion Homogenization Temperatures, Salinities, Isotope Compositions, and Gas Abundances from the Six Assemblages that Combine the Sandstorm-Kendall Ledge

Assemblage	$T_{h_{quartz,barite}}$ (°C)	NaCl fluid inclusions (wt %)	δD_{H_2O} fluid inclusions (‰)	$\delta^{18}O_{H_2O}$ fluid inclusions (calculated) (‰)	$CO_2 + H_2S + SO_2 + N_2$ (wt %)
(1) Ledge replacement quartz	est. 250–325		+3 to −54	−0.3 to −8.3	3.8
(2) Barite + sulfides	220–292	0.2 to 7.9	−7 to −102	+4.2 to −2.8	24.7
(3) Quartz + pyrite + barite	227	1.4 to 3.0	−29 quartz	−5.0	
(4) Quartz + barite + kaolinite breccia	257	3.4 to 6.0	−61 quartz	−5.8	
			−82 barite	−8.4	
(5) Vuggy quartz	248–255	0.3 to 3.0	−123 to −135	−7.1 to −9.6	12.4
(6) Lateral replacement quartz	est. 100–200		−58 to −137	−3.7 to −17.6	27.5

Data are summarized from Table 5

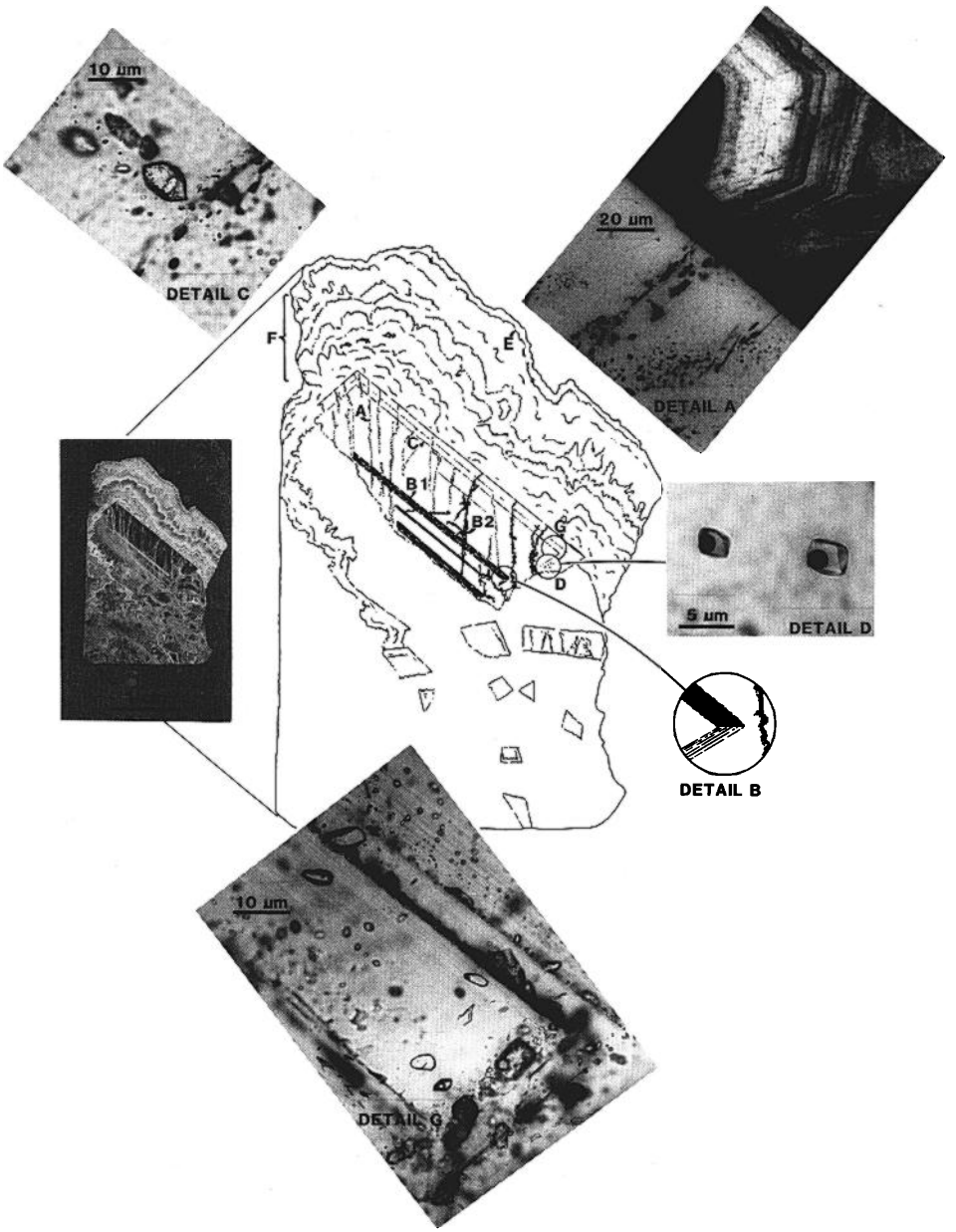

FIG. 7. Photograph, line drawings, and photomicrographs of a large (1.5-cm) barite euhedron of assemblage (2) attached to ledge replacement quartz (assemblage (1)) and an aggregate of fine-grained quartz and smaller barite euhedrons. Bands of quartz cover the large barite crystal. "A," "B1," "B2," "C," "D," and "G" lie within the large barite crystal; "E" and "F" refer to encrusting quartz. **A.** Fractures in barite containing pseudosecondary liquid-rich and vapor-rich fluid inclusions with $T_{h_{median}}$, liquid-rich $\cong$ 220°C. Some fractures cut planes of solid inclusions (B1 and C) and some transect the entire barite crystal but not encrusting quartz (detail A). **B.** Crystal growth plane (B1) and irregular fractures (B2) in barite containing black opaque solid inclusions, and a few pyrite euhedrons. Solid inclusions in growth planes are confined to 001 (detail B). **C.** Crystal growth planes (001, 210) in barite containing spindle-shaped to doubly terminated, partly sorted quartz crystals which range in size from <1 to ~30 mm (detail C). **D.** Primary fluid inclusions in barite (detail D) with $T_{h_{median}}$ = 249°C. **E.** Sparsely distributed pyrite euhedrons in outer bands of encrusting quartz. **F.** Rhythmic, plumose bands of fine-grained to microcrystalline quartz containing variable abundances of fluid and solid inclusions. **G.** Primary fluid inclusions and quartz crystals in barite growth planes (detail G).

quantitatively analyzed by microprobe using energy dispersive techniques, long counting times, and two RAP detectors. It is composed of about 53 percent carbon, 25 percent sulfur, 7 percent oxygen, and 5 percent iron with the balance (10%) inferred to be hydrogen.

TABLE 5. Homogenization Temperatures, Salinities, and Isotopic Data

Assemblage	Sample no.	Mineral	$T_{h(f.i.)}$[1] median	$T_{h(f.i.)}$[2] range	Salinity[2] (equiv wt % NaCl) (measured on quartz, barite)
Sandstorm-Kendall Ledge					
(1) Ledge replacement quartz	GFM85-1 (eqa)	Quartz	e250; 275		
	GFM85-3	Quartz	e250; 325		
	GF85-1 (eqb)	Quartz	e250; 275		
	GF85-3 (eq)	Quartz	e250; 275		
	GF82-2A	Quartz	218		
(2) Barite ± sulfides	GFM85-1B	Barite	292; 240–270	*20:* 280–305; *7:* 240–270	*27:* 0.3–2.3; 2.5–3.5; 4.0–4.7[3]
	GFM85-6	Barite	265	*15:* 255–270	
	GFM85-7	Barite	el 260	*14:* 255–275	*9:* 0.2–0.5
	GFM85-8	Barite	el 250	*25:* 235–265	
	GFM85-1A	Barite	249; 220	*13:* 240–265; *38:* 204–240	*12:* 0.3–2.6; 7.9
	GFH85-2	Barite	264; 243	*13:* 250–275; *13:* 230–250	
	GF82-2A, 2B	Barite	>260; 230	*11:* 260–280; *45:* 215–240	*17:* 0.2–0.7
(3) Quartz + pyrite + barite	GFM86-1A	Quartz	227; 217; 203	*11:* 220–235; *11:* 210–220; *6:* 200–210	*15:* 1.4–3.0
(4) Quartz + barite + kaolinite breccia	GFM85-1 (qtrAu)	Quartz	el 250		
	GFM85-1 (barAu)	Barite	257	*14:* 250–270	*13:* 5.3–6.0; 3.4–3.9[3]
(5) Vuggy quartz	GFM85-2	Quartz	el 240		
	GFM85-3 (lq)	Quartz	255; 237	*19:* 245–265; *13:* 230–245	
	GF85-1	Quartz	248; 233	*38:* 215–275; *33:* 210–245	*9:* 2.4–3.0
	GF85-3	Quartz	el 230	*8:* 220–235	*2:* 0.3–0.9
(6) Lateral replacement quartz	GFM86-10	Quartz	e200; 125; 100		
	GFM86-18	Quartz	e200; 125; 100		
	GFM86-19	Quartz	e200; 125; 100		
	GF87-3	Quartz	e200; 125; 100		
	GF87-40	Quartz	e200; 125; 100		
	GF87-41	Quartz	e200; 125; 100		
	GF87-42	Quartz	e200; 125; 100		
	GF87-43	Quartz	e200; 125; 100		
	GF87-44	Quartz	e200; 125; 100		
	GF87-48	Quartz	e200; 125; 100		
	GF87-49	Quartz	e200; 125; 100		
	GF87-50	Quartz	e200; 125; 100		
Alunite + pyrite	GFM85-1				
	GFM86-17				
	GF87-1				
	GF87-4				
Gypsum ± pyrite	GF85-5				
	GFM86-15				
	GF87-7				
	GF87-8				
Main district quartz	GF81-3	Quartz	385; 240–320; 200–230	*39:* 365–405; *28:* 240–320; *20:* 200–230	
	GF82-3	Quartz	≫260; 245; 224	*6:* 255–265; *29:*230–255; *18:* 220–230	
	GF87-1	Quartz	266[8]; e375	*34:* 255–275	
Unaltered pre-Tertiary rocks			$\delta^{18}O_{whole\ rock}$		
	GF87-54	Quartz monzonite, W of Columbia Mountain	8.6		
	GF87-59	Quartz monzonite, Vindicator Mountain	8.5		
	GF87-52	Palmetto shale, Columbia Mountain	17.2		
	GF87-60	Palmetto shale, Vindicator Mountain	24.8		

Temperatures used in the calculations are fluid inclusion homogenization temperature medians of the mineral analyzed. Fluid inclusion homogenization temperature medians ($T_{h_{f.i.}}$) and salinities were determined using microthermometry apparatus manufactured by SGE, Inc. Fluid deuterium compositions were determined by crushing mineral separates in vacuum and analyzing water released from fluid inclusions by mass spectrometry. Oxygen and sulfur isotope compositions were measured directly on mineral separates. Analytical errors: $\delta^{18}O_{quartz} \pm 0.1‰$; $\delta^{18}O_{barite} \pm 0.5‰$; $\delta D \pm 2‰$; $\delta^{34}S \pm 0.5‰$. Isotopic analyses are by Geochron Laboratories, Cambridge, Massachusetts

[1] Initial number in the column $T_{h(f.i.)}$ median = primary inclusions except for assemblages (1) and (6); all subsequent numbers = pseudosecondary

for Sandstorm-Kendall and Adjacent Ledge Assemblages

δD_{H_2O} (‰) (measured)	$\delta^{18}O_{quartz}$ (‰) (measured)	$\delta^{18}O_{barite}$ (‰) (measured)	$\delta^{18}O_{H_2O_{quartz\text{-}barite}}$ [4,5] (‰) (calculated)	$\delta^{34}S^{2}$ (‰) (measured on barite, pyrite)	$\delta^{34}S_{SO^{-2}}$ (‰) (measured on barite, alunite gypsum)	$T_{\delta^{34}S_{sulfate\text{-}sulfide}}$ [6] (calculated)
−24	3.5		−5.4; −4.3			
+3	5.1		−3.8; −0.94			
−12	7.5		−1.4; −0.33			
−54	0.6		−8.3; −7.2			
+627	3.0		−7.5			
−7		6.8	4.2	3.2	26.0	249
		4.5	0.9		28.4	
−72		7.1	3.3		26.9	
−84		1.4	−2.8		26.0	
−42		4.0	−0.2		24.7	
−102		4.1	0.5		27.2	278
−102		4.6	0.8	6.8	27.3	
−29	5.0		−5.0	1.6		
−61	3.1		−5.8			
−82		12.3	−8.4		27.2	
+18	2.3		−7.1			
−123; −115[7]	2.1		−6.5; −7.4			
−135			−9.6; −8.4			
−129	1.1		−8.7			
−135	6.8		−4.8; −10.9; −13.8			
−59	4.1		−7.5; −13.6; −16.4			
−124	7.7		−3.9; −10.0; −12.9			
−137[7]	7.9		−3.7; −9.8; −12.7			
−78	4.1		−7.5; −13.6; −16.4			
−88	5.7		−5.9; −12.0; −14.9			
	5.3		−6.3; −12.4; −15.3			
−64	4.3		−7.3; −13.4; −16.3			
−85	5.1		−6.5; −12.6; −15.5			
−100	2.9		−8.7; −14.8; −17.6			
−65	6.6		−5.0; −11.1; −14.0			
−58	3.2		−8.4; −14.5; −17.3			
				1.6	25.1	241
				−4.8	22.1	207
				5.4	9.3	1,074
				−0.9	15.0	356
					2.6	
				−3.9	23.7	200
					4.9	
					2.1	
−120	−0.1		−4.5; −6.3 to −9.4; −9.9 to −11.0			
−110	−1.0		−9.4; −10.1; −11.1			
−2	2.9		−5.3; −1.7			

inclusion populations; e = estimated; el = estimated from limited fluid inclusion homogenization temperature determinations or large range. [2]Numbers in italics represent number of analyses. [3]Pseudosecondary fluid inclusions. [4]$\delta^{18}O_{quartz\text{-}water}$ was calculated from the following equation, with T in °K: $10^3 \ln \alpha = 3.34\ (10^6\ T^{-2}) - 3.31$ (Matsuhisa et al., 1979); it should be noted that $\delta^{18}O_{quartz\text{-}water}$ is extrapolated to low temperatures indicated by fluid inclusion data. [5]$\delta^{18}O_{barite\text{-}water}$ was calculated from the equation, with T in °K: $10^3 \ln \alpha = 3.0\ (10^6\ T^{-2}) - 6.79$ (Friedman and O'Neil, 1977). [6]$T_{\delta^{34}S_{sulfate\text{-}sulfide}}$ was calculated from the equation, with T in °K: $10^3 \ln \alpha = 6.063\ (10^6\ T^{-2}) + 0.56$ (Ohmoto and Rye, 1979; Ohmoto and Lasaga, 1982). [7]Water recovered by thermal decrepitation. [8]Median homogenization temperature for fluid inclusions in quartz subhedrons in quartz monzonite

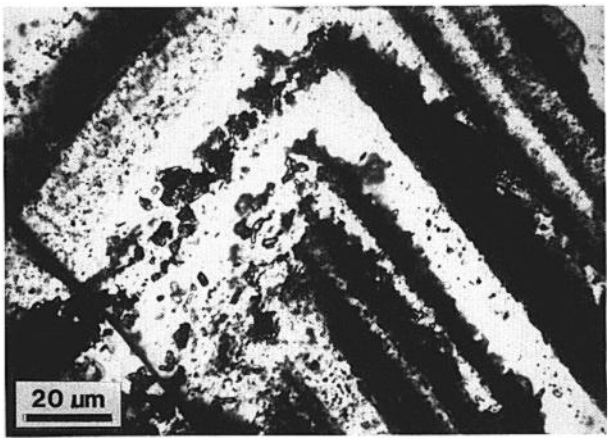

FIG. 8. Skewed distribution of entrained solid inclusions of quartz and organic compounds (?) in barite.

Ledge selvages

In rhyolite immediately adjacent to ledge replacement quartz (assemblage 1), feldspar-rich flow layers have been replaced by nearly 100 percent pink alunite or white pearly kaolinite (Fig. 2). Generally the widths of alunite and kaolinite-dominated selvages are 10 ft (3 m) or less. With increasing distance from a ledge segment montmorillonite in feldspar and biotite sites becomes more abundant, displacing both alunite and kaolinite. Montmorillonite-altered rocks are uniformly buff to off-white or light green in color, checked, and quite friable. Nearly all rocks within the area of Figure 2 contain some montmorillonite. There are only two small surface exposures in which feldspars and biotite in rhyolites are largely unaltered: ~400 ft (121 m) southwest from the Goldfield Consolidated Mines Company mill site, and 900 ft (272 m) north of the Conqueror shaft.

No alunite was observed in altered Milltown Andesite, perhaps because there are no ledges in Milltown Andesite in the area of Figure 2. The alteration assemblages in Milltown Andesite along strands of the Adams-Conqueror fault zone are kaolinite + quartz in the fault strands and light green montmorillonite ± quartz extending for >10 ft (>3 m) from the fault strands, as determined by X-ray diffraction analyses. The precursors of strongly altered rocks are usually identified by relict porphyritic texture, including the presence or absence of quartz phenocrysts.

The relative ages of quartz, alunite, kaolinite, and montmorillonite in the Sandstorm-Kendall area can only be partially determined. Ledge replacement quartz (assemblage 1) clearly formed before all other ledge assemblages as evidenced by the infilling of silicified and fractured rhyolite by all younger assemblages. Alunite and ledge replacement quartz apparently formed nearly contemporaneously as alunite + quartz replace rhyolite which consisted of up to 30 percent void space. Some replacement quartz may have been derived from alunitization (and kaolinization) of feldspars in rhyolite. The age of montmorillonite, which is always distal to both the alunite selvage and ledges, relative to alunite and ledge quartz is unclear. Kaolinite is the stable aluminum phase in the Sandstorm-Kendall ledge since it is a component of several ledge assemblages. It also flanks more ledge segments than does alunite in the area of Figure 2, suggesting that it partially replaced alunite after ledge replacement quartz (assemblage 1) was deposited.

In the main district the sequence of alteration assemblages flanking ledges is consistent regardless of the composition of the original rock. The assemblages include an outer chlorite-calcite-antigorite (propylitic) zone, a medial montmorillonite-illite-kaolinite-quartz (argillic) zone, and an alunite-quartz-sulfide inner zone (Harvey and Vitaliano, 1964; Ashley, 1974). Alunite is apparently younger than all other minerals except kaolinite which occurs in thin veins crosscutting quartz-alunite-altered rock as well as disseminated in rock matrices.

Fluid Inclusion Temperatures and Compositions from the Sandstorm-Kendall Ledge

Fluid inclusion homogenization temperatures and partial fluid chemical and isotopic compositions were determined in 31 samples in ledge replacement quartz (assemblage 1), barite of assemblages (2), (3), and (4), quartz of assemblages (3), (4), and (5), and lateral replacement quartz (assemblage 6). These data are summarized in Table 4. Homogenization temperatures and fluid salinities were measured using gas-flow microthermometry equipment manufactured by SGE, Inc. Fluid isotopic and gas compositions were obtained by mass spectrometry of fluid extracted from quartz and barite crushed in a vacuum. Although each mineral was cleanly separated for bulk gas and fluid isotopic analyses, fluid inclusions in ledge replacement quartz (assemblage 1) and lateral replacement quartz (assemblage 6) were too small for accurate temperature measurements and relative age assignments. Estimated depositional temperatures and temperature ranges for these assemblages and measured homogenization temperature modes for all other assemblages are given in Table 5.

Barite contains abundant, relatively large (10–50 µm), clearly visible fluid inclusions (Figs. 7 and 9). Primary inclusions occurring along growth planes generally fill negative crystals. Far more numerous pseudosecondary inclusions define fractures crosscutting growth planes; they mostly occupy long, prismatic cavities. The majority of the inclusions are gas rich or are completely filled with gas as determined by crushing in oil.

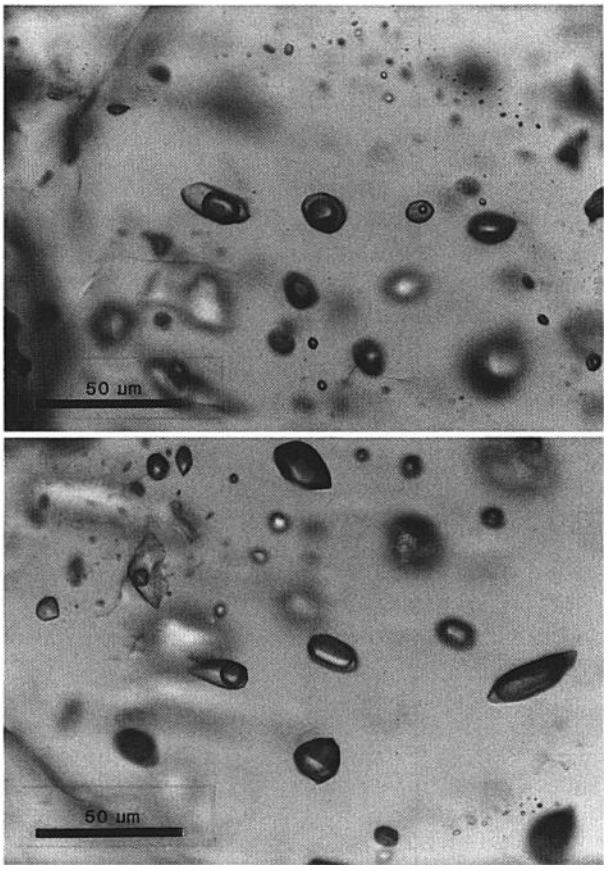

FIG. 9. Fluid inclusions in assemblage (2) barite containing highly variable phase ratios.

Repeated homogenization determinations on primary inclusions in barite gave a precision within 1° to 2°C at temperatures up to 280°C; no perceptible stretching occurred. Above 280°C decrepitation was frequently observed although some inclusions remained intact and apparently unstretched to temperatures of 310° to 320°C. Thus, limitations presented by fluid inclusions in barite mainly involved bulk fluid (isotopic and gas) analyses and, to a lesser extent, inclusion origin—problems encountered with virtually all other minerals.

Deuterium abundances in quartz and barite were measured directly on water extracted from fluid inclusions crushed in a vacuum. The $\delta^{18}O$ abundances were measured on quartz and barite residues after the water was extracted. These mineral analyses were converted to values for water in equilibrium with quartz or barite at the depositional temperatures indicated by fluid inclusion microthermometry. The mineral-water isotopic equilibrium equations used (Friedman and O'Neil, 1977; Matsuhisa et al., 1979) are given in the caption of Table 5.

Homogenization temperatures for primary fluid inclusions in barite were measured in eight samples from the Sandstorm-Kendall and adjacent ledges (Table 5). Homogenization temperature medians range from 230° to 292°C in assemblage (2), barite + sulfides, with barite from unoxidized samples from the Kendall mine having homogenization temperature medians of 230°, 249°, and 292°C. Barite in assemblage (4), quartz + barite + kaolinite breccia, has a homogenization temperature median of 257°C.

The interpretation of barite fluid inclusion temperatures and compositions is complicated by numerous planes of pseudosecondary inclusions, by the abundance of gas-rich inclusions, and by the capacity of barite to deform irreversibly by stretching at high temperatures (Ulrich and Bodnar, 1988). Primary inclusions isolated along growth planes were distinguished from pseudosecondary inclusions for temperature and salinity determinations, but bulk analyses of fluids extracted from entire crystals mixed fluid isotopic compositions (Table 5). Mixing of fluid inclusion populations is indicated by bulk gas analyses (Fig. 10 and Table 6) which display total gas concentrations ranging from about 4 to 29 wt percent. Several quartz and barite samples contain >10 wt percent CO_2 whereas no liquid CO_2 was observed in any inclusion as would be expected in a homogeneous population of this composition. CO_2, the most abundant species, and other gases were at least partially derived from the gas-rich pseudosecondary inclusions common among the several barite inclusion populations. Planes of these gas-rich inclusions apparently caused the highly variable gas analyses of barites.

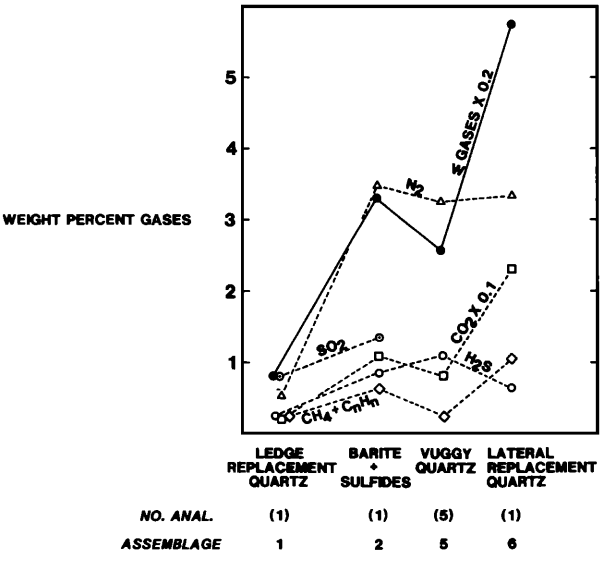

FIG. 10. Gas analyses, in weight percent, of fluid inclusions from assemblages comprising the Sandstorm-Kendall ledge. Data are from Table 5.

TABLE 6. Analyses (in wt and mole %) of Fluids in Fluid Inclusions in Quartz and Barite from the Sandstorm-Kendall Ledge

Sample no. assemblage	GF82-2q Ledge replacement quartz (1)		GF85-1 eqab Barite + sulfides (2)		GF85-1B Barite + sulfides (2)		GFM85-1b Barite + sulfides (2)		GFM85-7b Barite + sulfides (2)		GFM85-8b Barite + sulfides (2)		GF85-1 1q Vuggy quartz (5)		GFM85-10 Lateral replacement quartz (6)	
	Wt %	Mole %	Wt %	Mole %	Wt %	Mole %	Wt %	Mole %	Wt %	Mole %	Wt %	Mole %	Wt %	Mole %	Wt %	Mole %
H_2O	95.93	98.20	74.70	86.40	83.76	91.70	91.90	96.10	81.03	90.10	86.42	93.00	87.09	93.10	71.23	85.00
CO_2	2.07	0.867	15.59	7.37	12.11	5.43	6.13	2.62	11.72	5.33	8.80	3.88	8.09	3.54	23.53	11.50
CO	0.04	0.024	0.55	0.412	0.19	0.134			0.33	0.236	0.19	0.128	0.23	0.156	0.18	0.136
H_2S	0.26	0.138	1.49	0.910	0.59[3]	0.340	0.12[3]	0.064	0.95	0.557	1.01	0.576	1.10	0.620	0.67	0.420
SO_2	0.78	0.224	1.85	0.602		2.32			0.94	0.295						
N_2	0.65	0.426	5.79	4.30	3.30		1.62	1.09	3.77	2.70	3.07	2.13	3.24	2.23	3.34	2.56
H_2							0.006	0.057	0.010	0.120	0.002	0.018	0.018	0.177		
CH_4	0.02	0.018					0.013	0.015	0.194	0.243	0.006	0.008	0.091	0.109		
C_nH_m	0.25	0.098					0.21	0.085	1.06	0.422	0.47	0.219	0.15	0.042	1.06	0.405
	100.00	100.00	99.97	99.99	99.95	99.92	99.99	100.03	100.00	99.99	99.97	99.96	100.01	99.97	100.01	100.02
T°C gas equil.[1]		197[2]		184[2]		181[2]		261		258		254		302		165[2]

Gases were released by thermal decrepitation and analyzed by mass spectrometry (D.I. Norman, New Mexico Institute of Mining and Technology, Socorro, New Mexico)

[1] D'Amore and Panichi (1980)

[2] CH_4 and/or H_2 absent

[3] H_2S odor detected during sample preparation

A less precise depositional temperature for copper-arsenic minerals which occur with barite is derived from the thermal stabilities of enargite and luzonite. The enargite-luzonite transition is near 300°C but probably lies "below rather than above 300°C" according to Maske and Skinner (1971, p. 905). Luzonite is the low-temperature polymorph. The occurrence of both minerals at temperatures, in part, much less than 300°C, as indicated by fluid inclusion homogenization in coeval barite, suggests that enargite is metastable, that the inversion temperature is too high, or that Sb lowers the inversion temperature. Einaudi (1977) reports the coexistence of enargite and luzonite at Cerro de Pasco, Peru.

Barite fluid inclusion δD_{H_2O} values range from −7 to −102 per mil; $\delta^{18}O_{H_2O}$ values for assemblage (2) are −2.8 to +4.2 per mil. The barite fluid inclusion δD_{H_2O} value in the one sample from assemblage (4) is −82 per mil and the calculated $\delta^{18}O_{H_2O}$ is equal to +8.4 per mil. The relationships of various fluid and solid inclusions in barite, and of barite to earlier and later hydrothermal assemblages, in the Sandstorm-Kendall ledge are shown in Figures 6 and 7.

The homogenization temperature median for primary fluid inclusions in quartz of assemblage (3), quartz + pyrite + barite, is 227°C and measured fluid δD_{H_2O} and calculated fluid $\delta^{18}O_{H_2O}$ values are −29 and −5.0 per mil, respectively (Table 5). Homogenization temperature medians for primary fluid inclusions in quartz of assemblage (5) vuggy quartz, range from 230° to 255°C and fluid δD_{H_2O} and calculated fluid $\delta^{18}O_{H_2O}$ values range from +18 to −135 per mil and −6.5 to −9.6 per mil, respectively (Table 5).

Fluid inclusion δD_{H_2O} and calculated fluid inclusion $\delta^{18}O_{H_2O}$ values for ledge replacement quartz, assemblage (1), range from +3 to −54 per mil and from −1.4 to −8.3 per mil, respectively (Table 5). Fluid inclusion δD_{H_2O} and calculated fluid inclusion $\delta^{18}O_{H_2O}$ values for lateral replacement quartz, assemblage (6), range from −58 to −137 per mil and from −3.7 to −17.3 per mil, respectively, for the estimated depositional temperature range 200° to 100°C (Table 5). All isotopic data are plotted in Figure 11.

Fluid salinities, in equivalent weight percent NaCl (Potter et al., 1978), were determined for fluid inclusions in quartz and barite from assemblages (2), (3), (4), and (5). Salinities, reported in Table 5, range from 0.2 to 7.9 wt percent for all assemblages and from 0.3 to 4.7 wt percent in assemblage (2). Enough data to establish a δD-salinity trend were only collected for assemblage (2), barite ± sulfides (Fig. 12). Salinity of assemblage (2) fluid inclusions generally increases with D enrichment and the most saline, enriched samples are very close in composition to SMOW. Carbon dioxide clathrate was observed in several assemblage (2) inclusions. The most dilute fluids, measured in assemblage (2) and assemblage (5) (vuggy

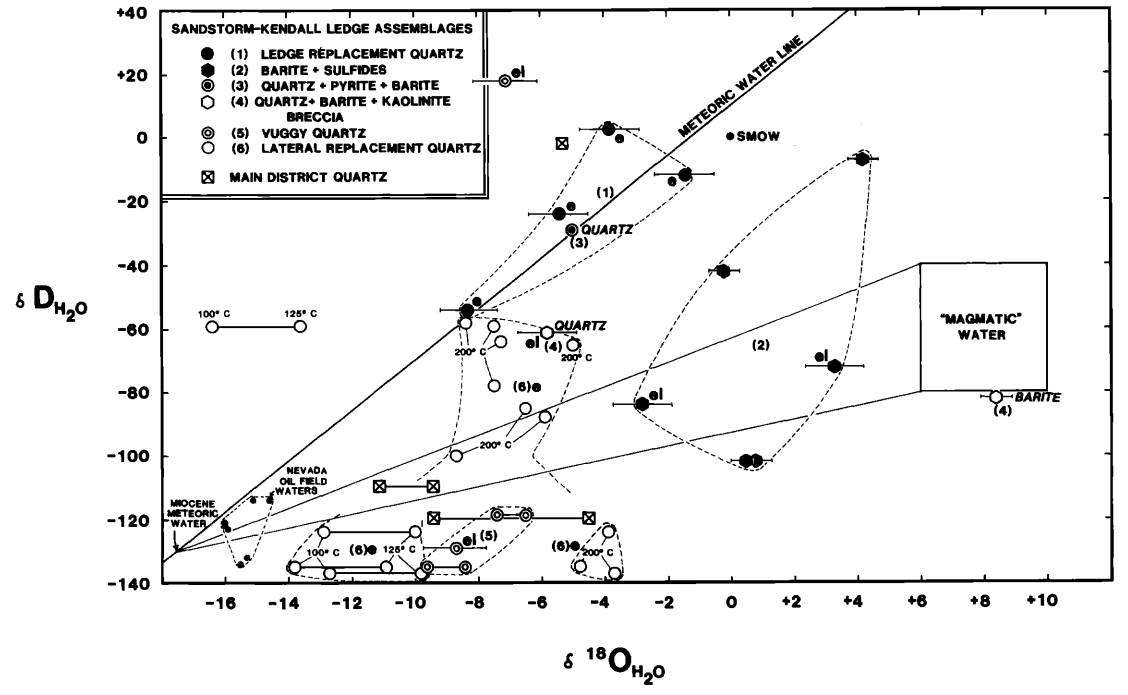

FIG. 11. δD_{H_2O} vs. $\delta^{18}O_{H_2O}$ plot of fluids from the six assemblages comprising the Sandstorm-Kendall ledge and from several main district ores. Data from Table 4. The meteoric water line, SMOW, magmatic water field, and Nevada oil field water isotopic compositions are included for reference. All $\delta^{18}O_{H_2O}$ values were calculated from $\delta^{18}O_{quartz,\ barite}$ as given in Table 4. The isotopic composition of Miocene meteoric water was estimated from assemblage (5) and (6) water. Symbol size and error bars encompass all analytical and measured temperature uncertainties. $\delta^{18}O_{H_2O}$ error bars represent a maximum of ±20°C. Oxygen isotope compositions for assemblage (6), lateral replacement quartz, and two main district ore fluids were calculated at several probable depositional temperatures (Table 4). Those data are linked by horizontal bars and enclosed by dashed lines. No fluid inclusion temperature data exist for assemblages (1) and (6). e = an estimated temperature used in positioning the data point; el = the data point which was positioned from limited fluid inclusion homogenization temperature determinations or large homogenization temperature range.

quartz) inclusions, have a δD value range of −7 to −135 per mil.

Vapor-rich inclusions with variable vapor/liquid ratios (Fig. 9) from each of the above assemblages have $NaCl_{equiv}$ concentrations that range from 0.0 to 7.9 wt percent, similar to liquid-rich inclusion salinities. None were filled with pure water as would be expected if the vapor-rich inclusions represented condensed steam. Boiling, however, must have occurred to some degree within the ledge-depositing fluid column, as high fluid temperatures (Table 5) and very thin cover (see "Discussion") could not conceivably preclude vapor exsolution from low-salinity fluids (Haas, 1971). However, most variable phase ratios in inclusions apparently are indicative of gases exsolving from the ore fluid during mineralization. Those gases are mainly CO_2, N_2, SO_2, and H_2S (Fig. 10 and Table 6). Separation of gases from the fluid may have concentrated dissolved salt(s) into the water-rich fluid, since many inclusions appear to be filled entirely with gas. Unrecognized CO_2 clathrate crystallization, or other dissolved gases, would have the same effect, leading to overestimation of salinities. Therefore, measured fluid salinities are maxima (Table 5).

Depth of Ledge Formation

By stratigraphic reconstruction Ransome (1909) estimated that about 300 ft (91 m) of premineralization rocks have been removed over main district ledges. Other estimates of postmineralization erosion are based on a weathering texture and radiometric ages of premineralization rocks and ore.

Spheroidal weathering of Milltown Andesite preserved by quartz replacement on Kendall Mountain (Figs. 2 and 13) suggests that the lateral replacement quartz (assemblage 6) of Kendall Mountain was precipitated essentially at the Miocene erosional surface. The early Miocene climate at Goldfield was more temperate and wetter than today, perhaps averaging as much as 20 to 25 in. (51–64 cm) of rainfall (Axelrod, 1957). The maximum depths below the surface where rocks develop spheroidal weathering, based on observations of road cuts in the western Sierra Nevada, which has a present climate not unlike that at Goldfield in the Miocene (Axelrod, 1968), are measured

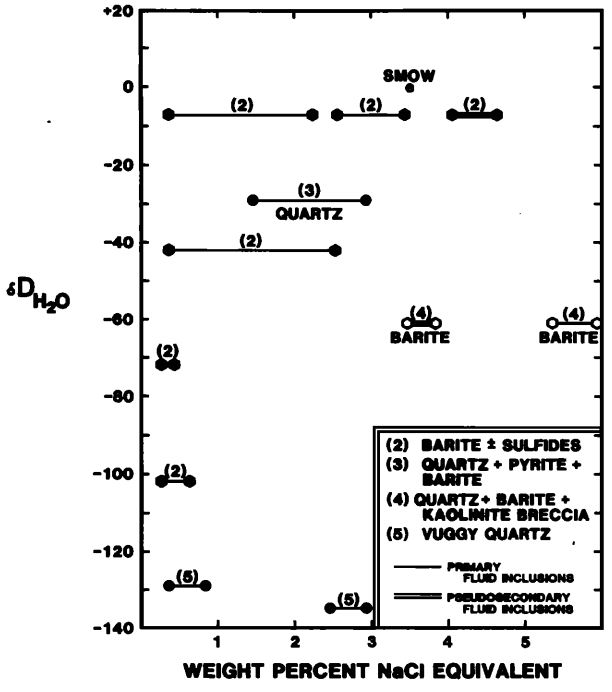

FIG. 12. Salinities, in equivalent weight percent NaCL, plotted against the deuterium content of fluids which deposited assemblages (2), (3), (4), and (5).

in a few tens of feet. The Buckhorn gold deposit in north-central Nevada formed in mid-Miocene basaltic andesites in and beneath graben-controlled lacustrine sedimentary rocks and subaerial sinter. Basaltic andesite pervasively altered to montmorillonite by ore-forming fluids prominently displays relict spheroidal weathering in pit walls at the mine that clearly took place no more than a few tens of feet below the paleosurface.

Lateral replacement quartz (replacing Milltown Andesite) covering Kendall Mountain is at the same elevation as the Sandstorm-Kendall ledge and other large areas of quartz-replaced rhyolite 1,000 ft (303 m) to the south-southwest (Fig. 2). No lithologic displacement by faults is evident between the two hydrothermally altered areas. Therefore, stratigraphic evidence in the Sandstorm-Kendall area suggests that gold-bearing ledges formed within a few tens to a few hundreds of feet below the surface, probably beneath mantos of silicified Tertiary volcanic rocks.

Other evidence for near-surface ledge development in the Sandstorm-Kendall area is supplied by radiometric ages of premineralization Milltown Andesite, porphyritic rhyodacite, and ledges at both Sandstorm-Kendall and in the main district. The average of radiometric ages for Milltown Andesite, 21.2 Ma, and the average age for Sandstorm-Kendall area ledge alunite, 21.7 Ma, are nearly identical (Table 1). They allow only minimal time between cessation of andesitic volcanism and onset of mineralization for erosion of Milltown Andesite and other premineralization rocks. Since porphyritic rhyodacite (dacite of Ransome, 1909), the likely heat source for main district mineralization (Ransome, 1909; Ashley and Silberman, 1976), has an average age of 20.6 Ma (Ashley and Silberman, 1976), very little erosion of premineralization rocks probably took place. From this reasoning present exposures of hydrothermal mineral assemblages in the Sandstorm-Kendall area cannot, therefore, be far below the Miocene paleosurface.

Sulfur Sources

Sulfur isotope compositions were determined for five barite samples from the barite + sulfides (2) and the quartz + barite ± kaolinite breccia (4) assemblages, three pyrite samples from the barite + sulfides (2) and the quartz + pyrite + barite (3) assemblages, four alunite samples from rhyolite and quartz monzonite replaced by alunite, quartz, and pyrite, and four gypsum samples. The $\delta^{34}S$ values in barite range from 24.7 to 28.4 per mil; in pyrite from 3.2 to 6.8 per mil; in alunite from 9.3 to 25.1 per mil; and in gypsum from 2.1 to 23.7 per mil (Table 5). The alunite $\delta^{34}S$ values are similar to those determined by Jensen et al. (1971) for hypogene main district alunites. Supergene alunite $\delta^{34}S$ values in the Jensen et al. (1971) study average $\sim 0.0(\pm 2.5)$ per mil, nearly equal to their $\delta^{34}S$ pyrite average of $-0.8(\pm 2.0)$ per mil.

Where pyrite and barite coexist, isotopic equilibrium temperatures calculated using the equations of Ohmoto and Rye (1979) and equilibrium data of Ohmoto and Lasaga (1982) are 249° and 278°C (Table 5). These isotopic temperatures are in general agreement with those derived from fluid inclusion homogenization in barite, which range from 257° to 292°C. Isotopic temperatures derived in the same

FIG. 13. Spheroidal weathering texture in Milltown Andesite preserved by silica replacement on Kendall Mountain.

manner for alunite + pyrite wall-rock alteration, and for gypsum + pyrite, range from 200° to 356°C (disregarding one calculated temperature of 1,074°C; Table 5). Assuming that sulfate-sulfide equilibrium in solution is attained in days to months at these temperatures (Ohmoto and Lasaga, 1982), barite-pyrite, alunite-pyrite, and gypsum-pyrite sulfur isotope thermometry at Goldfield gives reasonable depositional temperatures. Where alunite-pyrite isotopic data do not provide believable temperatures, isotopic disequilibrium must be assumed. Although no coexisting sulfide-sulfate pairs were analyzed, average $\delta^{34}S_{\text{alunite-pyrite}}$ reported by Jensen et al. (1971) in the main district gives T°C $\cong$ 312.

Speculative sources for both barium and sulfur in sulfates and sulfides in the Sandstorm-Kendall ledge center on the pre-Tertiary rocks beneath Goldfield, specifically Palmetto metasedimentary rocks which contain bedded and vein barite. Palmetto barites have been mined in Esmeralda County 18 mi (30 km) southwest and 67 mi (112 km) northwest from Goldfield (Papke, 1984) but have not been isotopically analyzed. Bedded barite $\delta^{34}S$ values elsewhere in Nevada range from −1.5 to +5.7 per mil (Tafuri, 1973; Mitchell, 1977; Rye et al., 1978; Radtke et al., 1980) and in the southeastern Mineral County Palmetto deposits, those closest to Goldfield, from 14.2 to 16.5 per mil (Tafuri, 1973). Assuming that Esmeralda County bedded barite has $\delta^{34}S$ values similar to southeastern Mineral County bedded barites, Sandstorm-Kendall $\delta^{34}S$ barite values require that Palmetto barite was hydrothermally enriched in $\delta^{34}S$ by ~10 to 12 per mil. Vein barites at Northumberland and Carlin, two gold deposits in Paleozoic rocks, are enriched by several per mil over the bedded barite range, a result of temperature-caused fractionation in hydrothermal fluids (Radtke et al., 1980). At Carlin, barite-sulfide isotope and fluid inclusion homogenization temperatures display a level of agreement similar to those in Table 5.

Gypsum intergrown with pyrite, and therefore assumed to be hypogene, from a mine dump 2,500 ft (758 m) southeast of the Sandstorm-Kendall ledge gives a plausible sulfur isotope temperature of 200°C (Table 5). This hypogene gypsum fills fractures in Milltown Andesite altered to quartz + montmorillonite + pyrite. Three other gypsum $\delta^{34}S$ values from the Sandstorm-Kendall area, MacMahon Ridge, and Black Butte average 3.2 ± 1.7 per mil and probably formed during low-temperature (surface) oxidation of pyrite which has similar average $\delta^{34}S$ values of ~5.0 ± 1.8 per mil (Table 5; Jensen et al., 1971). Gypsum is presently forming in dumps in the main district.

Jensen et al. (1971) suggest that sulfide sulfur in the main district with an average $\delta^{34}S_{\text{pyrite}}$ value of −0.8 per mil was derived from a Tertiary intrusion and that heavy sulfate sulfur was derived from oxidation of magmatic H_2S. At Sandstorm-Kendall, $\delta^{34}S$ values of near zero in pyrite and about 25 per mil in hypogene sulfates are also consistent with the derivation of sulfur from a magmatic source at the probable temperatures, sulfidation state, and oxidation state of fluid which formed the Sandstorm-Kendall ledge (Ohmoto, 1972; Ohmoto and Rye, 1979; Rye et al., 1988).

As long as SO_2 is a minor component, $\delta^{34}S_{H_2S} \cong \delta^{34}S_{\text{ore fluid}} \cong 0$ per mil, the assumed value for magmatically derived sulfur. However, up to 1.85 wt percent SO_2 was measured in fluid inclusions in quartz and barite of assemblages (1) and (2), representing as much as 75 wt percent of the sulfur gases present (H_2S and SO_2) in those samples (Table 6), although five other samples contained only H_2S. The H_2S-SO_2 fractionation is about 15 per mil at 300°C and 20 per mil at 400°C (Ohmoto and Rye, 1979). The $\delta^{34}S$ value in Sandstorm-Kendall ore fluid was therefore at least several per mil as reflected by an average $\delta^{34}S$ value of pyrite $\cong$ 5 per mil and the presence of significant SO_2 in fluid inclusions. Brimhall and Ghiorso (1983) demonstrated that Goldfield-like hydrothermal assemblages could result from thermal fluids containing subequal amounts of SO_2 and H_2S ($SO_2 \leq H_2S$).

Water Sources

Isotopic compositions of water which deposited the six assemblages that comprise the Sandstorm-Kendall ledge vary more widely than published data for any other ore deposit. Sources for the younger assemblage waters (5 and 6) are, in part, easily recognized, but the earliest hydrothermal phases precipitated from waters whose origin is not entirely clear.

Within the limits of analytical error no δD_{H_2O} values for assemblages (1), (2), (3), and (4) are greater than δD_{SMOW} and all are considerably enriched in D and ^{18}O relative to the values established for Miocene meteoric water (Fig. 12 and Table 5). This suggests that early Sandstorm-Kendall hydrothermal fluids could have been derived from isotopically modified seawater ("formation water") or mixtures of oceanic, pre-Miocene meteoric water and/or Miocene meteoric water. As used in this discussion pre-Miocene meteoric water is considered to have isotopic compositions that plot on the meteoric water line (MWL) of Figure 12. A possible source for the seawater component of assemblages (1) through (4) fluids is Ordovician sedimentary rocks of the Palmetto Formation which underlie the Tertiary section at Goldfield as well as much of southwestern Nevada (Albers and Stewart, 1972). However, the isotopic composition of Ordovician seawater apparently differed little from that of today (Taylor, 1979) and most likely never varied as much as the isotopic analyses of assemblages (1) through (4), regardless of latitudes and climates at which Palmetto sediments accumulated.

Deuterium analyses of assemblage (1) vary from meteoric water line and SMOW values, and the following mechanisms can be invoked to explain them: (a) increasing the estimated precipitation temperatures of assemblage (1) (and two other samples) from 250° to 275° or 325°C to enrich $\delta^{18}O_{H_2O}$ to values "below" the meteoric water line (Table 5), (b) climatic variations (temperature, sea level changes) in the early Miocene that shift the meteoric water line to more enriched deuterium and depleted ^{18}O values, (c) deuterium exchange with organic compounds or hydrogen-bearing gases, (d) deuterium partitioning by micropore (membrane) filtration by shales and clay minerals (Clayton et al., 1966; Fritz and Frappe, 1982; Kharaka and Carothers, 1986), (e) deuterium exchange with clay minerals at elevated temperatures (White et al., 1973), (f) release of deuterium-depleted water from hydrated minerals, (g) exchange between ^{18}O-depleted CO_2 and a limited volume of pore fluid; silicate hydration and clay crystallization from restricted pore fluids, and (h) incorporation of isotopically heavy water from closed basins.

The effects of alternatives (b) through (h) cannot be directly evaluated. The small amounts of hydrogen gases measured in fluid inclusions and the high W/R ratio implied by the close positioning of some water isotopic compositions to the meteoric water line suggest that even complete isotopic exchange with pore fluids or hydrogen-bearing phases would have a marginal effect on hydrothermal fluid deuterium compositions. Boiling concentrates deuterium and heavy oxygen in residual fluid, thereby elevating δD values to higher than meteoric water line deuterium, but it is difficult to envision the independent fractionation required not to simultaneously enrich ^{18}O to meteoric water line or greater values. Alternative (a) offers a relatively simple explanation that eliminates deuterium fractionation for assemblage (1), and alternative (b) is supported by average global water $\delta^{18}O$ value $\cong$ 1.2 per mil at 20 Ma (Williams et al., 1988).

Assemblage (2) water, considerably enriched in ^{18}O relative to pre-Miocene meteoric water (Fig. 12 and Table 5), apparently exchanged heavy oxygen with wall rocks at elevated temperatures to a greater degree than other early assemblage waters. Paleozoic rocks beneath Goldfield are highly enriched in ^{18}O with $\delta^{18}O$ values up to 24.8 per mil (Table 5). Some assemblage (2) water may contain an increment of magmatic water. Fluid salinities decrease with deuterium depletion (Fig. 13) suggesting dilution by meteoric water(s). Since barite occurs in Palmetto Formation rocks and most ledge barite is in assemblage (2), deep circulation of assemblage (2) water is implied.

The variable isotopic compositions of assemblage (3) and (4) waters are represented by only three analyses. They are indicative of either weakly to unexchanged pre-Miocene meteoric water, pre-Miocene meteoric water highly enriched in ^{18}O, or magmatic water (Fig. 12; Table 5). The large difference in $\delta^{18}O_{H_2O}$ values between coeval quartz and barite of assemblage (4) suggests that the $\delta^{18}O_{barite}$ value was inherited largely from Palmetto Formation bedded barite.

Isotopic compositions of assemblage (5) water and of two main district fluid inclusion waters can be explained as Miocene meteoric water moderately enriched in ^{18}O by exchange with Tertiary and pre-Tertiary wall rocks at elevated temperatures. One water sample is so highly enriched in D and depleted in ^{18}O that no reasonable temperature correction will place the composition on or to the right of the meteoric water line. The validity and significance of this analysis are uncertain.

Similar to assemblage (1) water, temperature estimates were used to calculate the isotopic compositions of assemblage (6) water. These estimates, 100°, 125°, and 200°C (Fig. 12; Table 5) were derived from the following reasoning. Assemblage (6) formed at or near the paleosurface at lower temperatures than earlier, deeper ledge assemblages because convective cooling and mixing with Miocene ground water thermally buffered assemblage (6) water. Also, 200°C temperatures are required to position some water compositions below the meteoric water line.

The isotopic compositions of assemblage (6) water are diverse and fall into two groups. One group of analyses from Kendall Mountain surface samples of silicified andesite represents Miocene meteoric water that has exchanged oxygen with wall rocks at low temperatures. The second group represents pre-Miocene meteoric water that has also exchanged oxygen with wall rocks, probably at temperatures approaching 200°C. Several analyses may be mixtures of meteoric and magmatic water. Samples in the second group are from the Kendall Mountain trench that cuts silicified Milltown Andesite (Fig. 5) and from pervasively silicified Sandstorm rhyolite and andesite at the northern extremity of the Sandstorm-Kendall ledge. The stratigraphic positions of the analyzed samples indicate that subsurface silicification of andesite was accomplished by pre-Miocene meteoric and possibly magmatic water at a temperature of about 200°C. Surface samples, those at or near the paleosurface (Fig. 13), were silicified by Miocene meteoric water at lower temperatures. On Kendall Mountain the interface between Miocene and pre-Miocene meteoric water and magmatic water was apparently no more than a few tens of feet below the paleosurface.

Discussion

Several lines of evidence are consistent with the rapid emplacement of a high-level heat source that

sponsored hydrothermal mineralization of the Sandstorm-Kendall ledge:

1. Depositional temperatures of ~220° to 290°C for ledge assemblages (2), (3), and (4), the gold-bearing assemblages, are abnormally high for the shallow depths of precipitation—hundreds of feet below the paleosurface based on stratigraphic reconstruction, alteration assemblages, and preserved spheroidal weathering. Assemblage (1) depositional temperatures may have exceeded 300°C.

2. The depositional temperatures define very high temperature gradients, as much as degrees Celsius per foot within and between ledge assemblages.

3. Ledge sediments, internal ledge brecciation, preferentially entrained solid inclusions in barite growth planes, oriented copper sulfosalt encrustations on barite crystals, gas-rich fluid inclusion populations, and the probable metastable coexistence of enargite + luzonite at T < 300°C, in conjunction with very high temperature gradients, indicate that the mineralizing fluid of assemblages (2), (3), and (4) degassed and boiled violently and experienced turbulent flow in open fissures within hundreds of feet below the paleosurface.

4. Hydrogen and oxygen isotopes of water show that earlier and deeper gold mineralizing fluid, that which deposited assemblages (1), (2), (3), and (4), was derived from pre-Tertiary metasedimentary rocks and possibly magma beneath Goldfield. Miocene meteoric water comprised the bulk of fluid that deposited the youngest assemblages, (5) and (6), essentially at the paleosurface.

5. Magmatically derived gases, particularly H_2S and SO_2 (Whitney, 1984) exolved during decompression of the mineralizing fluid (point 3 above), caused extensive low pH hydrolysis of wall rocks, producing alunite and kaolinite adjacent to the Sandstorm-Kendall ledges and sulfates and sulfides within the ledge. According to fluid inclusion analyses these volatiles comprise as much as 3.34 wt percent of ledge-forming fluids at Sandstorm-Kendall (Table 6).

Since ledges in the main district are essentially coeval with rhyodacite, latite, and andesite (Ashley and Silberman, 1976), subvolcanic intrusions or diapirs of these rocks may have supplied thermal energy for hydrothermal circulation throughout the Goldfield district. A reconstructed portion of the Sandstorm-Kendall ledge (Fig. 14) summarizes key evidence pertaining to ledge evolution.

A major problem that arises from the above interpretation concerns the presence of liquid water, or a weakly saline aqueous fluid, as the major component of the ledge-depositing fluid. Ledge temperatures exceeded 220°C at very shallow depths beneath the paleosurface, as defined by hydrothermal mineral assemblage reconstruction and spheroidal weathering.

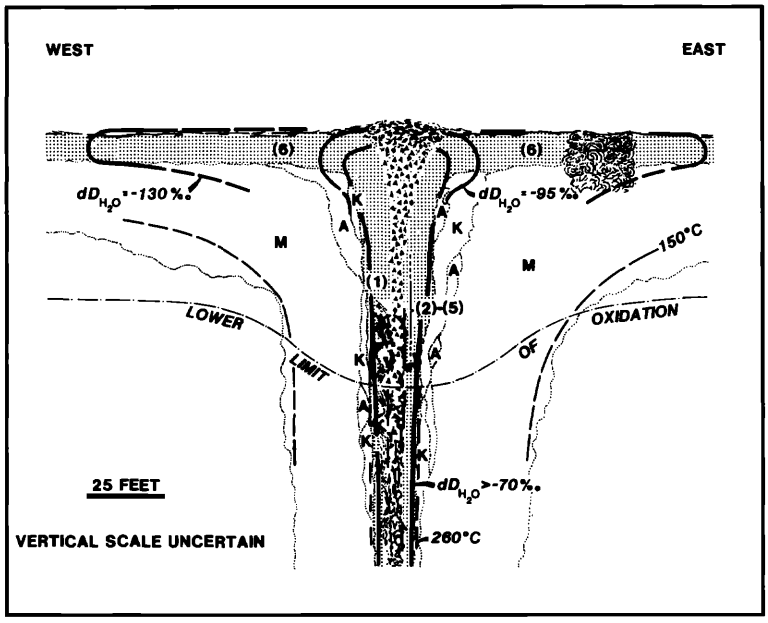

FIG. 14. Diagrammatic west-east section of a reconstructed Sandstorm-Kendall ledge segment showing hydrothermal assemblages, δD_{H_2O} contours, isotherms, and postmineralization oxidation. Ledge assemblages (1) through (6) are patterned. Wall-rock alteration assemblages: A = alunite + quartz ± pyrite, K = kaolinite + quartz ± pyrite, M = montmorillonite + quartz ± pyrite. Samples from assemblages (1) and (6) are shown in Figure 6 and are discussed in the text; δD and isotherms are from data in Table 5. Thin dashed lines are isotherms; thick dashed lines contour δD_{H_2O}.

According to the data of Haas (1971) hydrostatic depths of 790 to 2,772 ft (240–840 m) are required for liquid composed of 95 percent water and 5 wt percent NaCl to remain liquid at temperatures of 220° to 290°C, respectively. Less saline liquid in this temperature range requires greater depths, as would water containing even small amounts of CO_2 (Bodnar et al., 1985). Fluid inclusion examination and analyses show that Sandstorm-Kendall mineralizing fluid contained large amounts of dissolved gases (Fig. 10 and Table 6), and fluid (CO_2) may have approached 10 wt percent.

This difficulty may be resolved in several ways:

1. The depth of cover over ledge assemblages which average 250°C could be increased by as much as 1,390 ft (420 m). Given the essentially equal ages of the host rocks and ledges, the Sandstorm-Kendall ledge would therefore have been deposited within a landform more than 1,000 ft higher in elevation than Kendall Mountain, clearly an implausible explanation by itself.
2. Kendall Mountain along Kendall Wash (Fig. 2) could have been downfaulted by more than 1,000 ft after mineralization. There is no surface evidence for such faulting and 1,000 ft of displacement would expose other district lithologies. The maximum thickness of Milltown Andesite and the Sandstorm Formation are 200 and 700 ft thick, respectively (Ransome, 1909), and less in the Sandstorm-Kendall area.
3. Ledge depositional temperatures could have been systematically overestimated because of a variable liquid/vapor ratio in the fluid inclusions, particularly in barite. The average thermal gradient of boiling, low-salinity aqueous solutions in the temperature range 220° to 290°C is approximately 33 ft/°C (Hass, 1971) and even slight temperature misestimates of a few degrees implicate hundreds of feet of cover.
4. The bottom of spheroidal weathering could have been at a depth of hundreds rather than tens of feet.
5. An increment of lithostatic confining pressure could have been present during ledge formation.
6. A combination of the above mechanisms could be utilized.

None of these alternatives is a sole satisfactory explanation for a 250°C, low-salinity aqueous solution near the paleosurface. Although combining alternatives (1), (2), and (3) may marginally contribute to increasing cover over the Sandstorm-Kendall ledge during deposition, lithostatic pressure is the only alternative that can be geologically justified. The evidence for fluid expansion cited above permits confining pressures of ledge-depositing fluids that are much higher than hydrostatic pressure at the same elevation. The vapor (confining) pressure for low-salinity aqueous solution at 250°C is about 39 bars (Haas, 1971). At 300 ft below the surface maximum hydrostatic pressure for a low-salinity aqueous solution is about 9 bars (Haas, 1971), indicating that a strong pressure differential existed within the Sandstorm-Kendall ledge regardless of adjustments to the elevation of the paleosurface.

Relation of the Sandstorm-Kendall Area to the Main District

Gold production from the Sandstorm and Kendall mines constituted <1 percent of the Goldfield district total. The relevance of the Sandstorm-Kendall ledge formation to ore deposition in the main district, where >95 percent of the production occurred, has obvious importance. The Sandstorm-Kendall ledge is amenable to the collection of a variety of data that are useful in the reconstruction of hydrothermal evolution. In contrast, the fine-grained, structurally complex main district ores and ledges, for the most part, do not yield such information. Therefore, comparisons are based only on limited observations made within the main district and on the reports by Ransome (1909) and Ashley (1974).

Wall-rock alteration assemblages at Sandstorm-Kendall appear to be consistent with those in the main district even though main district ledges formed in rhyodacite and latite. The six assemblages comprising the Sandstorm-Kendall ledge, however, do not occur in the main district. Barite and coarsely crystalline vuggy quartz are virtually absent in main district ledges. Metallic phases unknown or uncommon at Sandstorm-Kendall, famatinite ($\sim Cu_3\ Sb_{0.5}\ As_{0.5}\ S_4$, Table 2), bismuthinite, goldfieldite, and gold tellurides (Table 2), are a significant component of some main district high-grade ores. In the main district, high-grade ore zones generally occur in brecciated portions of ledges, often within ledge flexures a few hundred feet below the surface. Rich near-surface ore consists of spectacular bands of gold, sulfides, and sulfosalts encrusted on breccia clasts of silicified volcanic rocks. Deep ore consists primarily of quartz and copper sulfosalts with inclusions of gold in narrow tabular veins that cut clay-altered latite and dacite. Below 500 ft (152 m) the quartz content of the ledges decreases markedly making them difficult to distinguish from altered wall rock. Ore was apparently mined to >1,000 ft (303 m) below the surface. Quartz in deep ore from the Little Florence mine dump has a fluid inclusion population that homogenizes at T > 300°C (sample GF81-3, Table 5). Near-surface, high-grade ore from the Sandstorm-Kendall area is quartz + barite + kaolinite breccia (assemblage 4), situated in interstices of ledges; a copper-rich assemblage similar to deep main district ore has not been encountered.

Ore zones and alteration assemblages at the Summitville gold deposit in southwest Colorado are similar to those at Goldfield (Steven and Ratte, 1960; Stoffregen, 1987), particularly within the upper several hundred feet of the deposits. Near-surface ore mineralogy at Summitville, including gold, pyrite, enargite-luzonite, and kaolinite, corresponds closely to the assemblages comprising the Sandstorm-Kendall ledge, although hypogene covellite and sulfur at Summitville have not been reported at Goldfield. High-grade "breccia pipes" at Summitville consist of gold, kaolinite, barite, and vuggy quartz clasts and mineralogically resemble assemblage (4) in the Sandstorm and Kendall mines. The deep chalcopyrite + tennantite association at Summitville has not been found at Goldfield, although exploration drilling has taken place to greater depths at Summitville than at Goldfield.

Goldfield and Summitville are the best-known representatives of a class of Au + Cu ± Ag deposits that are characterized by locally high gold and copper grades, ore zones of irregular geometry, "vuggy" silica, copper arsenic sulfides, and intense kaolinite-alunite alteration of Tertiary host rocks. Similar deposits, also known as "enargite-gold" and "acid sulfate deposits," occur in the Walker lane area of Nevada and California, and in scattered Tertiary volcanic rock provinces elsewhere in the world. Others occur above or adjacent to porphyry copper deposits. Goldfield and Summitville are associated with coarsely porphyritic rhyodacite and quartz latite (respectively) intrusions that are situated on caldera ring fractures and are coeval with gold-copper mineralization.

The Sandstorm-Kendall deposits, satellitic to the main district mines at Goldfield, exhibit most features common to other enargite-gold deposits (Ashley, 1982). In detail, however, high, near-surface ore fluid temperatures, abundance of sulfur gases in ore fluid, and disparate water sources have not been measured for other similar deposits although they might be expected. Further comparisons must await the collection of detailed data both in the Goldfield main district and elsewhere.

Acknowledgments

Appreciation is extended to ASARCO Inc. for encouraging this study and for permission to publish the results. Comments by two *Economic Geology* reviewers greatly improved the original manuscript and were much appreciated.

November 22, 1988; August 14, 1989

REFERENCES

Albers, J. P., and Stewart, J. H., 1972, Geology and mineral deposits of Esmeralda County, Nevada: Nevada Bur. Mines Geology Bull. 78, 80 p.

Ashley, R. P., 1973, Fission-track ages for premineralization volcanic and plutonic rocks of the Goldfield mining district, Esmeralda and Nye Counties, Nevada: Isochron/West, no. 8, p. 25–30.

—— 1974, Goldfield mining district: Nevada Bur. Mines Geology Rept. 19, p. 49–66.

—— 1982, Occurrence model for enargite-gold deposits: U. S. Geol. Survey Open-File Rept. 82–795, p. 144–147.

Ashley, R. P., and Silberman, M. L., 1976, Direct dating of mineralization at Goldfield, Nevada, by potassium-argon and fission-track methods: ECON. GEOL., v. 71, p. 904–924.

Axlerod, D. I., 1957, Late Tertiary floras and the Sierra Nevada uplift: Geol. Soc. America Bull., v. 68, p. 19–46.

—— 1968, Tertiary floras and topographic history of the Snake River basin, Idaho: Geol. Soc. America Bull., v. 79, p. 713–734.

Brimhall, G. H, Jr., and Ghiorso, M. S., 1983, Origin and ore-forming consequences of the advanced argillic alteration process in hypogene environments by magmatic gas contamination of meteoric fluids: ECON. GEOL., v. 78, p. 73–90.

Clayton, R. H., Friedman, I., Graf, D. L., Mayeda, T. K., Meents, W. F., and Shimp, N. F., 1966, The origin of saline formation waters, I. Isotopic compositions: Jour. Geophys. Research, v. 71, p. 3869–3882.

D'Amore, F., and Panichi, C., 1980, Evaluation of deep temperatures of hydrothermal systems by a new gas geothermometer: Geochim. et Cosmochim. Acta, v. 44, p. 549–556.

Einaudi, M. T., 1977, Environment of ore deposition at Cerro De Pasco, Peru: ECON. GEOL., v. 72, p. 893–924.

Friedman, I., and O'Neil, J. R., 1977, Compilation of stable isotope fractionation factors of geochemical interest: U. S. Geol. Survey Prof. Paper 440-KK, 12 p.

Fritz, P., and Frape, S. K., 1982, Comments on the ^{18}O, ^{2}H and chemical composition of saline groundwaters on the Canadian Shield, *in* Perry, E. C., Jr., and Montgomery, C., eds., Isotopic studies of hydrologic processes: Dekalb, Illinois, Northern Illinois Univ. Press, p. 57–63.

Haas, J. L., Jr., 1971, The effect of salinity on the maximum thermal gradient of a hydrothermal system at hydrostatic pressure: ECON. GEOL., v. 66, p. 940–946.

Harvey, R. D., and Vitaliano, C. J., 1964, Wall-rock alteration in the Goldfield district, Nevada: Jour. Geology, v. 72, p. 564–579.

Jensen, M. L., Ashley, R. P., and Albers, J. P., 1971, Primary and secondary sulfates at Goldfield, Nevada: ECON. GEOL., v. 66, p. 618–626.

Kharaka, Y. K., and Carothers, W. W., 1986, Oxygen and hydrogen isotope geochemistry of deep basin brines, *in* Fritz, P., and Fontes, J. C., eds., Handbook of environmental isotope geochemistry: New York, Elsevier, p. 305–360.

Maske, S., and Skinner, B. J., 1971, Studies of the sulfosalts of copper I. Phases and phase relations in the system Cu-As-S: ECON. GEOL., v. 66, p. 901–918.

Matsuhisa, Y., Goldsmith, J. R., and Clayton, R. N., 1979, Oxygen isotope fractionation in the system quartz-albite-anorthite-water: Geochim. et Cosmochim. Acta, v. 43, p. 1131–1140.

Mitchell, A. W., 1977, Geology of some bedded barite deposits, north central Nevada: Unpub. M.S. thesis, Univ. Nevada-Reno, 58 p.

Ohmoto, H., 1972, Systematics of sulfur and carbon isotopes in hydrothermal ore deposits: ECON. GEOL., v. 67, p. 551–578.

Ohmoto, H., and Lasaga, A. C., 1982, Kinetics of reactions between aqueous sulfates and sulfides in hydrothermal systems: Geochim. et Cosmochim. Acta, v. 46, p. 1727–1745.

Ohmoto, H., and Rye, R. O., 1979, Isotopes of sulfur and carbon, *in* Barnes, H. L., ed., Geochemistry of hydrothermal ore deposits, 2nd ed.: New York, Wiley Intersci., p. 509–567.

Papke, K. G., 1984, Barite in Nevada: Nevada Bur. Mines Geology Bull. 98, 125 p.

Potter, R. W., II, Clynne, M. A., and Brown, D. L., 1978, Freezing

point depression of aqueous sodium chloride solutions: ECON. GEOL., v. 73, p. 284–285.
Radtke, A. S., Rye, R. O., and Dickson, F. W., 1980, Geology and stable isotope studies of the Carlin gold deposit, Nevada: ECON. GEOL., v. 75, p. 641–672.
Ransome, F. L., 1909, Geology and ore deposits of Goldfield, Nevada: U. S. Geol. Survey Prof. Paper 66, 258 p.
Rye, R. O., Shawe, D. R., and Poole, F. G., 1978, Stable isotope studies of bedded barite at East Northumberland Canyon in Toquina Range, central Nevada: U. S. Geol. Survey Jour. Research, v. 6, p. 221–229.
Rye, R. O., Bethke, P. M., and Wasserman, M. D., 1988, Diverse origins of alunite and acid-sulfate alteration: Stable isotope systematics [abs.]: Geol. Soc. America Abstracts with Programs, v. 20, p. A333.
Schieber, J., and Katsura, K. T., 1986, Sedimentation in epithermal veins of the Bohemia mining district, Oregon, USA: Interpretation and significance: Mineralium Deposita, v. 21, p. 322–328.
Searls, F., 1948, A contribution to the published information on the geology and ore deposits of Goldfield, Nevada: Nevada Bur. Mines Geology, v. 42, 42 p.
Steven, T. A., and Ratte, J. C., 1960, Geology and ore deposits of the Summitville district, San Juan Mountains, Colorado: U. S. Geol. Survey Prof. Paper 343, 70 p.
Stoffregen, R. E., 1987, Genesis of acid-sulfate alteration and Au-Cu-Ag mineralization at Summitville, Colorado: ECON. GEOL., v. 82, p. 1575–1591.
Tafuri, W. J., 1973, A geochemical study of the barite deposits of Mineral County, Nevada: Unpub. M.S. thesis, Univ. Nevada-Reno, 69 p.
Taylor, H. P., Jr., 1979, Oxygen and hydrogen isotope relationships in hydrothermal mineral deposits, *in* Barnes, H. L., ed., Geochemistry of hydrothermal ore deposits, 2nd ed.: New York, Wiley Intersci., p. 236–277.
Ulrich, M. R., and Bodnar, R. J., 1988, Systematics of stretching of fluid inclusions II: Barite at 1 atm confining pressure: ECON. GEOL., v. 83, p. 1037–1046.
White, D. E., Barnes, I., and O'Neil, J. R., 1973, Thermal and mineral waters of nonmeteoric origin, California Coast Ranges: Geol. Soc. America Bull., v. 84, p. 547–560.
Whitney, J. A., 1984, Volatiles in magmatic systems: Rev. Econ. Geology, v. 1, p. 155–176.
Williams, D. F., Lerche, I., and Full, W. E., 1988, Isotope chronostratigraphy: Theory and methods: New York, Academic Press, 345 p.